A Hybrid Design of integrated Silicon (Si) solar cell with Guided Mode Resonance Filter (GMRF)

By

Muhammad Sohaib Badar

NUST-2013-61520-MCES-64113-F

Supervised by

Dr. Muhammad Rizwan Saleem (Adjunct Faculty)

U.S Pakistan Center for Advanced Studies in Energy (USPCAS-E)

National University of Sciences & Technology (NUST)

H-12, Islamabad, 44000, Pakistan

May, 2017

A Hybrid Design of integrated Silicon (Si) solar cell with Guided Mode Resonance Filter (GMRF)

By

Muhammad Sohaib Badar

NUST-2013-61520-MCES-64113-F

Supervised by

Dr. Muhammad Rizwan Saleem (Adjunct Faculty)

A thesis submitted in conformity with the requirements for the degree of

MASTER of SCIENCE in

ENERGY SYSTEMS ENGINEERING

U.S Pakistan Center for Advanced Studies in Energy (USPCAS-E)

National University of Sciences & Technology (NUST)

H-12, Islamabad, 44000, Pakistan

May, 2017

THESIS ACCEPTANCE CERTIFICATE

Certified that final copy of MS/MPhil thesis written by Mr. Muhammad Sohaib Badar (Registration No. NUST-2013-61520-MCES-64113-F), of U.S Pakistan Center for Advanced Studies in Energy (USPCAS-E) has been vetted by undersigned, found complete in all respects as per NUST Statues/Regulations, is free of plagiarism, errors, and mistakes and is accepted as partial fulfillment for award of MS/MPhil degree. It is further certified that necessary amendments as pointed out by GEC members of the scholar have also been incorporated in the said thesis.

Signature: _____

Name of Supervisor: Dr. Muhammad Rizwan Saleem

(Adjunct Faculty)

Date: _____

Signature (HoD): _____

Date: _____

Signature (Dean/Principal): _____

Date: _____

Certificate

This is to certify that the work in this thesis has been carried out by **Mr. Muhammad Sohaib Badar** and completed under our supervision at U.S Pakistan Center for Advanced Studies in Energy (USPCAS-E), National University of Sciences & Technology (NUST), Islamabad, Pakistan.

Supervisor

_____

Dr. Muhammad Rizwan Saleem
(Adjunct Faculty)
USPCAS-E
NUST, Islamabad

GEC member # 1

_____

Dr. Parvez Akhter
USPCAS-E
NUST, Islamabad

GEC member # 2

_____

Dr. Majid Ali
USPCAS-E
NUST, Islamabad

GEC member # 3 (External)

_____

Dr. Iftikhar Hussain Gul
School of Chemical and
Materials Engineering
(SCME),
NUST, Islamabad

HoD-USPCAS-E

_____

Dr. Zuhair S. Khan
USPCAS-E
NUST, Islamabad

Principal/ Dean

_____

Dr. Muhammad Bilal Khan
USPCAS-E
NUST, Islamabad

In the Name of Allah, the Most Beneficent, the Most Merciful

Dedication

I dedicate my thesis work to my beloved *parents*, my younger *brother* and *sister*.

Acknowledgements

First and foremost, I would like to express my sincere gratitude to my supervisor Prof. Dr. Muhammad Rizwan Saleem (adjunct faculty) for his continuous support, patience, motivation, enthusiasm, and immense knowledge throughout this research work. His guidance helped me in all the time of research and writing of this thesis. I am very grateful to Dr. Rizwan for having the faith in me to give me the liberty and space to conduct my research without any limitations and constraints.

Besides my supervisor, I would like to thank the rest of my GEC committee: Dr. Parvez Akhter, Dr. Majid Ali, and Dr. Iftikhar Hussain Gul for their encouragement, insightful comments and moral support.

I would like to express my sincerest gratitude towards Prof. Dr. Mohammad Bilal Khan and the entire faculty at USPCAS-E for their unwavering cooperation and never ending support. Without their presence this dissertation might never have been completed in a timely manner. In addition, a big shout out to my colleagues at NUST who have been very supportive on the day to day matters of the research phase and for making life at NUST interesting.

Finally, I must express my very profound gratitude to my parents and to my younger brother and sister for providing me with unfailing support and continuous encouragement throughout my years of study and through the process of researching and writing this thesis. This accomplishment would not have been possible without them.

Abstract

The objective of this thesis work is to improve the optical absorption of silicon (Si) solar cell by increasing solar absorption. For this purpose, a hybrid design of silicon (Si) solar cell is designed with guided-mode resonance filter (GMRF) to increase absorption efficiency. The GMRF is a resonant waveguide grating (RWG) structure, which increases the resonant field and enhances the propagation path for light within the cell material. Light confinement in silicon (Si) solar cells through GMRF structure is theoretically demonstrated. The GMRFs are designed in Fourier Modal Method (FMM) using regression algorithm. A hybrid design of Si solar cell with GMRF is designed in the Finite-Difference Time-Domain (FDTD) software. The waveguide grating structure is defined by designing a grating structure in fused silica (SiO_2) material coated with a high index thin layer of amorphous titanium dioxide (TiO_2) material. The designed waveguide grating structure exhibits a 100% resonance reflectance response at a particular resonance wavelength λ_r.

One of the possible optimized designed parameters for the waveguide grating structure are: grating period d = 316 nm, grating grooved height h_g = 120 nm, structural-line width w = 205 nm, fill factor f = 0.65, refractive index of SiO_2 n_s = 1.45, refractive index of TiO_2 n_t = 2.385, thickness of TiO_2 layer t = 50 nm, angle of incidence $\theta_i = 18^o$, and resonance wavelength λ_r = 632.8 nm (Helium-neon laser), whereas, the realizable designed parameters for Si solar cell are: refractive index of Si material N = 3.882 + i(0.019) at resonance wavelength λ_r = 632.8 nm, cell thickness T = 500 nm. Compared to a planar Si solar cell, approximately 38% enhancement in the optical absorption is achieved over the 550-750 nm wavelength range for a GMRF enabled Si solar cell. This improvement in optical absorption of hybrid device structure inspires the application of Guided-Mode Resonance (GMR) effect in solar cells where increased absorption efficiency is a key demand. The GMRF enabled solar cells possesses the capability to indicate a new hybrid-design concept to improve the optical absorption. An appropriate optimization of grating design parameters in simulation guides to effective hybrid device operation. The theoretical explanation demonstrates the prospective of appropriate designed GMRF characteristics in silicon (Si) solar cells.

Keywords: Guided-Mode Resonance Filters (GMRFs), enhanced light absorption, silicon solar cells, Fourier Modal Method (FMM), Finite-Difference Time-Domain (FDTD)

Contents

List of Figures

List of Tables

List of abbreviations and symbols

RETs	Renewable Energy Technologies
RE	Renewable Energy
PV	Photovoltaic
UV	Ultraviolet
AM0	Air Mass 0
AM1.5	Air Mass 1.5
GMRF	Guided Mode Resonance Filter
GMRFs	Guided Mode Resonance Filters
GMR	Guided Mode Resonance
TE	Transverse Electric
TM	Transverse Magnetic
RWG	Resonant Waveguide Grating
1D	One-Dimensional
2D	Two-Dimensional
3D	Three-Dimensional
IPV	Impurity Photovoltaic
IB	Intermediate Band
QW	Quantum Well
ARC	Antireflection Coating
AR	Antireflection
RMS	Root Mean Square
FMM	Fourier Modal Method

FDTD	Finite Difference Time Domain
FWHM	Full Width at Half Maximum

Symbols

O_3	Ozone
O_2	Oxygen
CH_4	Methane
N_2O	Nitrous oxide
H_2O	Water
CO_2	Carbon dioxide
V_{oc}	Open-circuit voltage
J_{sc}	Short-circuit current density
eV	Electron volts
Si	Silicon
GaAs	Gallium Arsenide
Ge	Germanium
InAs	Indium Arsenide
Ag	Silver
a-Si:H	Hydrogenated Amorphous Silicon
SiO_2	Fused silica
TiO_2	Titanium dioxide

Author's list of Journal Publications

***Journal Article**

Muhammad Sohaib Badar, Muhammad Rizwan Saleem

Improved absorption efficiency of silicon (Si) solar cells through Resonant Waveguide Gratings (RWGs) – A hybrid design of RWG and Si solar cell

Published in "Optik-International Journal for Light and Electron Optics"

Available online: 4th October 2016

Year: 2017

Volume: 128

Pages: 50-56

*Attached as annexure I

Chapter 1

INTRODUCTION

The energy coming from the Sun in the type of heat and radiant light is known as the solar energy. Depending on energy conversion technologies, solar energy can be converted into different useable energy types. In this thesis work, we focus on the conversion of sunlight into electrical energy by solar photovoltaic (PV) technology. The power transformation efficiency of solar cell depends on the absorption of light coming from the Sun. There are many limitations that effect the power transformation efficiency of a solar cell. In literature, many techniques have been evolved to increase the efficiency of solar cells. Here, we report an efficient light trapping mechanism named as "guided-mode resonance filter (GMRF)" to increase the probability of light absorption in silicon (Si) solar cells. The GMRF structure traps the incoming sunlight and enhances the optical absorption of Si solar cell. A brief introduction about the history and working principle of GMRF structures is presented in this chapter. Recent developments in efficiency improvement techniques of solar cells is also reviewed, whereas, an overview of improvement of light absorption in thin-film Si solar cells through photonic devices is also described in this chapter.

1.1 Solar Energy

Renewable Energy Technologies (RETs) have gained interest day by day in the world energy mix in the past two decades [1]. In 2012, almost 13.2% of the total world energy supply was based on renewable energy resources and this percentage increased up to 18% in 2013, nearly 5% expansion from 2012 [2]. The advances in research and development of renewable energy technologies (RETs) have shown that with all developed technologies, renewable energy resources i.e., wind energy, biofuels, ocean energy (tidal and wave energy), solar photovoltaic technologies and solar thermal technologies could perform a vital part in the world energy mix in upcoming decades [3]. Amongst all renewable energy (RE) resources, solar energy is the most abundant and clean energy source that can contribute maximum in the overall energy production of renewable resources [4, 5]. In our solar system, the Sun has been the continuous source of

solar energy, well beyond the existence of the Earth and expectation to shine till by the end of this world. Hence, the continuous availability of this energy source shows that solar energy has a huge potential to contribute in overall world energy production to serve for energy consumers [6]. However, because of high capital cost, less efficiency and reliability issues [7], solar energy shares less percentage of its huge potential in useful energy production.

Solar radiations/energy coming from the sun can be converted into different useful energy productions i.e., electrical, thermal and chemical energy [8]. In this research work we focus on the first one, which is defined as the photovoltaic (PV) energy transformation. A photovoltaic (PV) device or solar cell comprises of two terminals named as; *Anode* and *Cathode*. When sunlight falls on such device it excites the electron-hole pairs inside the active layer of the cell and creates a potential difference between the two terminals [9]. The light incident on the solar cell is physically composed of energy packets of photons; in 1905 **Albert Einstein** observed that electrons were radiated due to absorption of light quanta (photons) through a solid (preferably metal) substance. The sunlight coming from sun is in the form of irradiations can be approximated by a black body held at a temperature of 6000 K emitting as per **Planck's distribution**. While reaching at the surface of earth, such radiations interfered by different atmospheric layers, present in earth's atmosphere which eventually weakens the strength of sunlight based irradiance. Almost 25% of the component of sunlight is scattered, reflected and absorbed by the atmospheric layers and rest of the 75% component reaches directly towards the earth's surface [10]. This direct component of sunlight eventually takes part in the transformation of light energy into electrical energy by solar cells. In visible and Ultraviolet (UV) region of solar spectrum, light is absorbed by different gaseous molecules present in atmosphere like ozone (O_3), oxygen (O_2), methane (CH_4) and nitrous oxide (N_2O). Similarly, light is absorbed by water vapors (H_2O) in mid-infrared and by carbon dioxide (CO_2) in far-infrared region [11]. The comparison of solar spectrum irradiation densities among outside atmospheric layer (represented by AM 0), on the earth's surface (represented by AM 1.5G) and black body radiation at 6000 K is shown in Figure 1.1. The curve represented by AM 1.5 G depicts the standard reference spectrum in photovoltaic, under the specified atmospheric conditions at an angle of incidence 48^o [12].

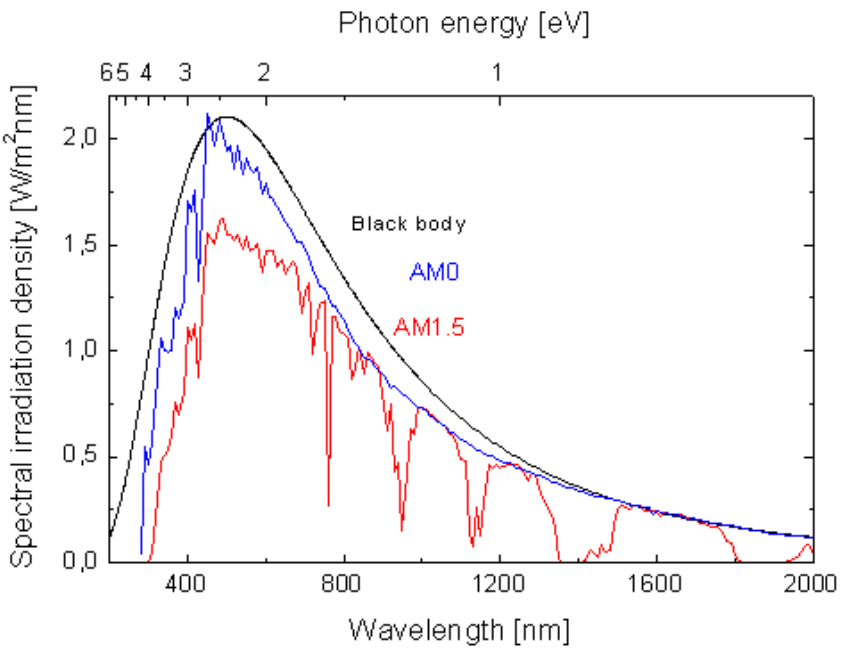

Figure 1.1: Graphical representation of solar spectrum irradiation densities; (AM 0 shows the blue curve for spectral irradiation density of outside atmospheric layer, AM 1.5 shows red curve for earth's surface and black curve shows black body radiation at 6000 K) [12].

1.2 Model and working principle of solar cell

A photovoltaic (PV) cell is usually defined by a semiconductor p-n junction. A p-n junction is formed by the integration of a n-type semiconductor material (doped with pentavalent impurity) and p-type semiconductor material (doped with trivalent impurity). These n-doped and p-doped semiconductor materials consist of charge carriers i.e., electrons and holes, respectively. By recombination factor and diffusion of charge carriers, a depletion region is formed in between the p-n junction and an electric field occurs due to donors and acceptor ions in this regime. At equilibrium state, this electric field provides a drift force to counter the diffusion force to prevent any charge flow in depletion region, as demonstrated in Figure 1.2.

The major component of photovoltaic cell is its forbidden energy band gap [13], if a photon of energy (hv) greater than or equal to that of forbidden energy band gap (E_g) strikes over the surface of solar cell then a free electron-hole pair (also named as exciton) is induced in space charge region of a p-n junction solar cell. This free electron-hole pair has enough energy to jump out of the depletion region to take part in conduction process, the free electron will move towards anode and free hole will move towards cathode terminal of solar cell. Figure 1.3 represents the energy band diagram of a p-n junction solar cell under illumination.

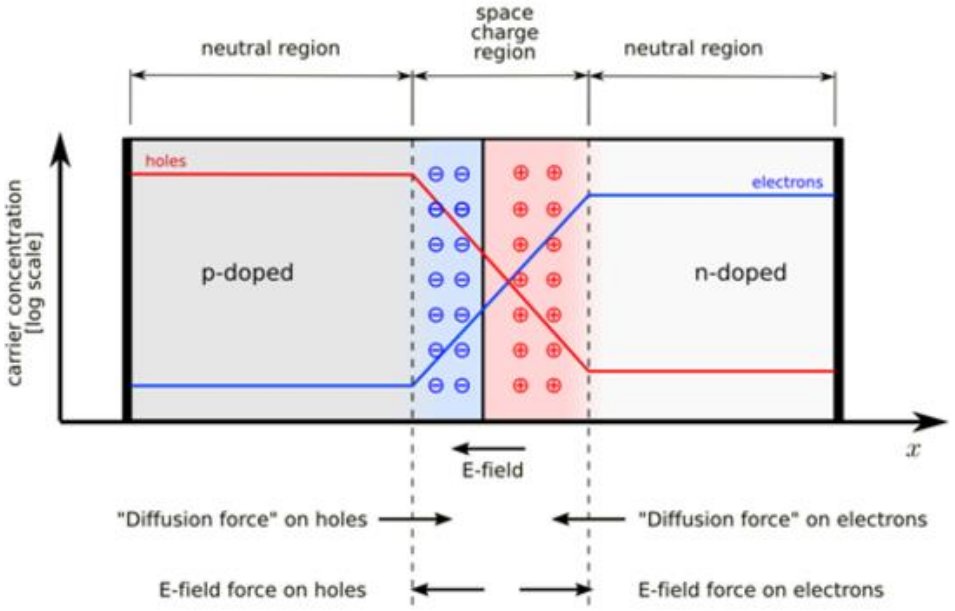

Figure 1.2: The schematic view of a p-n junction solar cell at equilibrium [14].

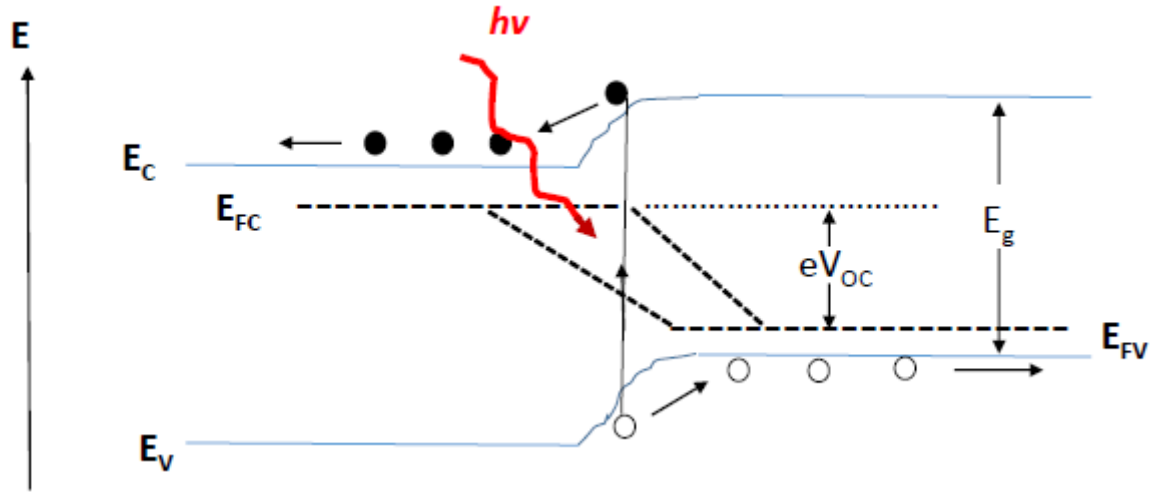

Figure 1.3: Energy band diagram of a p-n junction solar cell when strikes with a photon of energy ($hv \geq E_g$).

After the emission of photons from the p-n junction the charge carriers i.e., electron or hole will recombine. Hence, the open circuit photo voltage V_{oc} is given by;

$$eV_{oc} = E_{FC} - E_{FV}, \qquad (1.1)$$

where, e represents the elementary charge, E_{FC} and E_{FV} are quasi-fermi levels of energy for conduction and valence bands, respectively [15].

1.3 Power conversion efficiency and limitations in standard cell

Power conversion efficiency of a standard PV device or a single p-n junction solar cell is defined as a function of the forbidden energy band gap. Hence, photons coming in the incident light must have energy value greater than or equal to the value of forbidden energy gap to excite electrons from valance band to conduction band of solar cell [16]. Whereas, an excited electron-hole pair loses its energy quickly due to improper thermalization. Hence, the power conversion efficiency of a standard solar cell is restricted up to 44% through this loss. Another important limitation in conversion efficiency is recombination loss or factor; this loss can be controlled by using semiconductor materials with high life-times for the photo-generated charge carriers [17].

In 1961, **Shockley** and **Queisser** shown that recombination process in solar cells are radiative in nature [18]. Hence, the limitations on the operation of a solar cell can be derived from the symmetry between the absorbed and emitted radiations during radiative recombination. The value of the maximum photo current can be calculated by the difference between absorbed and emitted radiation. In this way, Shockley and Queisser were able to define an efficiency limit for a single p-n junction solar cell (at 6000 K) irradiated by a black body up to 31%, having a band gap of 1.3 eV (electron volts). This decrement in efficiency limit than the previous value of 44% is because of voltage decreases at the contact and junction of solar cell. Owing to such loss the output voltage of solar cell becomes lower than band gap potential [19]. Figure 1.4 depicts the limitations in the performance of a standard solar cell, process 1 indicates the thermalisation loss, process 2 and 3 indicates junction and contact voltage loss respectively and process 4 indicates the recombination loss [17].

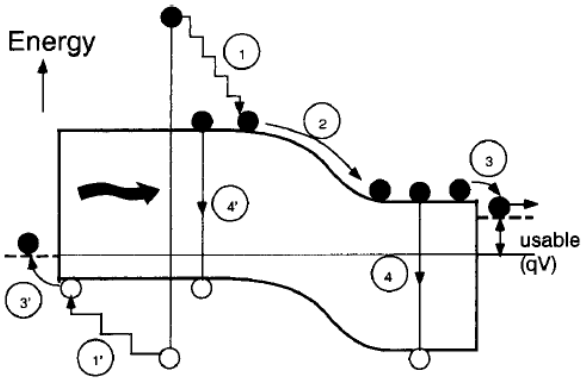

Figure 1.4: Processes for the limitation in the performance of a p-n junction solar cell: (a) 1-thermalisation loss, (b) 2 & 3-junction and contact voltage loss, and (c) 4-recombination loss [17].

1.4 Advances in solar cell concept

Solar cell technology is gaining interest as the most effective renewable energy technology to convert sunlight into electrical energy [20]. There are various forms of solar cells, for example, wafer-based silicon, thin-film silicon and tandem solar cells [21–23]. Such categorization of solar cells depends on the fabrication processes and required materials one aims for [16]. The wafer-based silicon solar cells are basically single crystalline or polycrystalline silicon solar cells and they belong to first generation category of solar cells. They are very much high in cost and have high efficiency limit up to 25% with an energy band gap of 1.1 eV [24]. Thin film solar cell technology belongs to second generation solar cells; they are cheap in cost in contrast to first generation solar cells and have low efficiency. However, during recent advances in thin film solar cell technology, their efficiency reached up to 20% [25].

Whereas, third generation solar cells have come up with more economical and efficient solar cell technologies i.e., multi-junction or tandem solar cells. Tandem solar cells are basically a combination of multiple cells with distinct energy band gaps; this approach enhances the probability of photon absorption in multi-junction solar cells with distinct energy values [26]. The cells are stacking in such a manner that cell with greater band gap will be on the top, photons with greater energy absorbed in uppermost cell and low energy photons will continue to absorb in cells with lower band gaps. Efficiency of these multi-junction cells depend on the number of cells in the stack arrangement, almost 86.8% efficiency has been evaluated for an infinite stack of separately operated cells. However, with limited number of cells in stack almost 41% and 51% efficiency values have been calculated for double and triple junction tandem solar cells, respectively [27]. Similarly, other advance concepts like multiple electron-hole pair per photon, hot carrier cells, multiband and impurity photovoltaic cells, and thermo photovoltaic and thermo photonic devices are also the part of third generation solar cells [17]. All these advanced techniques are developed to boost the performance of a solar cell for an efficient transformation of sunlight into electrical energy.

It has been found that the energy transformation efficiency of a solar cell strongly depends on the absorption coefficient of the light within the material [28]. The absorption coefficient can be increased using efficient light-trapping techniques to refine the performance of a solar cell [29]. The light coming from the sun can be easily confined within the cell by designing proper

photonic nanostructures, which will reduce the losses of reflection and scattering of light on the surface of the cell [30]. In this research work we have proposed a hybrid design of silicon (Si) solar cell with Guided Mode Resonance Filter (GMRF) to enhance the optical absorption of a silicon solar cell.

1.5 Historical Background

The phenomenon of diffraction of light had been introduced since the time of Newton, but in 1786 Rittenhouse, first time practically shown the concept of diffraction grating made from hairs separated by two fine screws' threads [31]. Later on, in 1902, Wood experienced quick variations in intensity of light reflected by metallic gratings with respect to little variations in incident angle and wavelength of incident light [32]. During an experimental work, Wood observed that when the metallic grating structure is illuminated by a TM polarized light, the diffracted spectrum of the grating structure showed quick growth in light intensity by a factor of ten in a wavelength interval "smaller than the space among the grating lines". These irregularities in diffracted spectrum were named as ***Wood's anomalies*** [32]. Lord Rayleigh, in 1907, described a theoretical analysis on Wood's grating structure, and observed that at particular wavelengths Wood's anomalies correlate with the new propagating diffraction orders appear from the grating structure at the grazing incidence eventually redistributed the total power in various diffraction orders quickly [33].

Rayleigh had considered a pure conducting grating material in his study, whereas, Fano in 1941, considered gratings made of lossy metal material [34]. During this study, he discovered two different types of anomalies: a Rayleigh-type, distinguished by a "sharp peak" in the diffracted spectrum, and a second one he defined as being "diffuse", distinguished by a maximum and minimum in diffracted spectrum [35]. During his experimental work, Wood had observed these anomalies only for TM (i.e., electric field is perpendicular to grating lines) polarized light, but later Palmer had shown that if gratings are of good depth, anomalies will also happen for the TE (i.e., electric field is parallel to grating lines) polarized light [36]. According to a new theoretical approach adopted by Hessel & Oliner in 1965 [37], Wood's anomalies are defined as the guided waves rather than the scattered waves and because of these guided waves assisted by the grating a resonance phenomenon occurred which is basically the second type of anomaly. These guided waves are leaky in nature because of complex wave numbers [37].

The grating structures were not only made from metals but also non-metallic or dielectric materials can be used for this purpose. In 1973, Neviere *et al*., had shown diffraction of light through non-metallic grating structures in his theoretical studies. These proposed non-metallic grating structures were designed by dielectric waveguides covered with corrugated photo-resist. These theories had clearly shown that when these dielectric waveguide grating structures were illuminated by incident light then at specific incident angle, a resonant response was shown for both TE [38] and TM [39] polarized incident lights that is due to the excitation of guided modes in the waveguide. In 1985, through experimental work, Mashev & Popov had revealed a resonant reflectance response in the zeroth order diffracted reflected wave due to the excitation of leaky modes in a waveguide grating structure [40].

In 1989, Bertoni *et al*., presented a dielectric slab structure created by sequential square bars of variable refractive indices. They showed that total reflection or total transmission of light could be acquired at different frequencies for the structure. They elaborated this concept by the excitation of guided modes through the structure, which re-radiated along the structure and combined directly with the reflected and transmitted light. When re-radiated light and reflected light waves were in phase matching condition then a strong reflection occurred, otherwise a strong transmission occurred [41]. Whereas, the phases were frequency dependent, the reflection displayed a (resonant) frequency selective behavior. In 1990, Gale *et al*., described through their experimental work that the dielectric grating structures showed highly efficient resonant reflectance response in the visible region, highly applicable in security and anti-counterfeiting systems [42].

In the last decade of 20^{th} century, Wang & Magnusson had worked on the sub-wavelength dielectric waveguide grating structures. They indicated in their various research articles that incident light waves diffracted in both forward and backward directions through dielectric grating structure, a 100% energy exchange occurred between these forward and backward diffracted waves over specific wavelength ranges due to the coupling effect between the propagating diffracted waves and leaky waveguide modes [43–48]. In their research work, they defined such resonant response from waveguide grating structure as “Guided Mode Resonance Filters (GMRFs)” and proposed different applications for GMRFs, for example, laser cavity mirrors, polarizer, tunable filters and electro-optic switches [45]. In 1996, Peng & Morris

proposed in their research that these resonant waveguide grating structures not only designed in one dimensional pattern, but also feasible in two dimensional pattern [49]. They revealed in their research work that two dimensional resonant waveguide grating structures showed two resonance peaks in reflectance spectrum when a plane light wave was incident on the structure, as compared to a one dimensional structure [50].

In 1997, Sharon, Rosenblatt & Friesem introduced a basic ray picture model to demonstrate a reflectance response at resonance, due to the complete destructive interference at transmission side and complete constructive interference at reflection side of a waveguide grating structure [51]. They had also shown in their experimental work the fabrication of semiconductor based resonant waveguide grating devices [52]. Fan & Joannopoulos presented a three-dimensional photonic crystal theory in 2002, to examine the temporary response of reflection and transmission of light through two-dimensional resonant waveguide grating structures. In their theory, they revealed that two-dimensional structures support two kinds of guided modes, one is conventional guided modes having very long life times and do not couple with the far field, and second are named as guided resonances that couples with the far field and result in short life time [53].

The concept of GMRF was originated by Wood, and because of this invention he introduced a new field of research in science of physics. Later, the progress in this field invented a concept of resonant waveguide grating structures quite efficient to show resonance reflectance response in the narrow wavelength bands. Such resonant waveguide grating structures were known by different technical names in the literature like, GMRFs, photonic crystal slabs, or photonic crystal resonant reflectors. In this work, we have referred this concept by guided mode resonance filters (GMRFs) and its application in photovoltaics.

1.6 Guided Mode Resonance Filter (GMRF)

The guided mode resonance filter (GMRF) is defined as a periodic dielectric grating structure which enhances the resonant field by coupling the incident light to the leaky mode of the waveguide of the grating for filtering applications. In other words, a diffraction grating with periodic modulation of refractive index can generally be called as a GMRF [54, 55]. Materials like metals, semiconductors and dielectrics can be used to fabricate these diffraction gratings [56–58]. When these diffraction gratings are exposed to an incident plane wave then it diffracts

into multiple diffraction orders i.e., diffracted plane waves will propagate in different directions. Guided Mode Resonance (GMR) represents a narrow peak in the spectral response of a waveguide grating structure related to the 100% energy trade between transmitted and reflected waves. Guided Mode Resonance (GMR) effect occurs when one of the diffracted waves from the waveguide grating structure is phase matched with a leaky waveguide mode [43, 45]. Due to the periodic modulation of waveguide grating structure, the guided-modes are leaky in nature; hence a sharp resonance peak will occur at a specific wavelength and angle of incidence of the incident plane wave [59]. At defined optical parameters, a sharp resonance peak of 100% can be obtained in reflectance or transmittance spectra.

In this research work we have proposed the application of GMR effect in silicon (Si) solar cells. The GMRF is a Waveguide Grating Structure which enhances the resonant field and elongates the propagation path for light within the Si solar cell material. The phase matching phenomenon of grating structure, guides the incident light into multiple resonances in the device, ultimately improving the possibility of light absorption due to enhancement in propagation length.

1.6.1 GMRF Structure

The simplest structure of a GMRF comprises of a one dimensional (1D) grating structure over a substrate layer as shown in the Figure 1.5. This single layer grating structure is acting as a waveguide medium, having greater effective refractive index value as compared to refractive indices of the substrate and cover. The waveguide layer can also be modified by adding one or more homogeneous layers in between the gating layer and the substrate. Figure 1.5 shows that when a plane light wave of wavelength λ is incident over a GMRF structure then it splits into multiple diffraction orders. While, the diffracted waves are reflected backward and transmitted forward. When one of the diffracted waves satisfy the phase matching condition, then guided mode resonance effect will occur in the waveguide grating structure [45, 60]. The direction of these reflected and transmitted diffracted waves in 1D-grating structure is calculated by the following fundamental grating equation [61].

$$n_{\mathrm{g}} \sin \theta_{\mathrm{m}} = n_{\mathrm{c}} \sin \theta_{\mathrm{i}} + m\lambda/d \,, \qquad (1.2)$$

where, d represents the grating period, λ represents the wavelength of incident plane wave, θ_i represents incident angle of plane wave, θ_m denotes the angle of diffraction, m = 0, ±1, ±2, ±3, ……. is the order of diffraction. The refractive index distribution for GMRF structure should be like $n_g > n_s > n_c$, where n_g is the refractive index of grating structure periodically distributed along the x-axis, n_c and n_s indicates the refractive indices of cover medium (normally air) and the substrate, respectively.

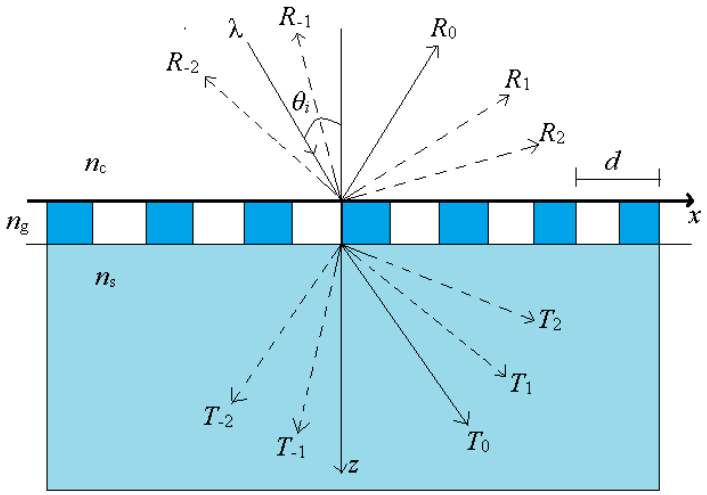

Figure 1.5: Schematic view of GMRF structure with reflected and transmitted waves [62].

1.6.2 Working principle of GMRF

The theory of operation of GMRF structure is established on excitation of leaky waveguide modes. When plane light waves are incident on the grating structure as shown in Figure 1.5, the incoming light wave couples with the waveguide mode by diffraction on the grating and resonance occurs; the resonance wavelength depends on the phase matching element of the grating layer. The effective mode propagation constant β for the evanescent diffracted wave at the phase matching condition is given by the equation [63];

$$\beta = k_0(\mathrm{n_c}\sin\theta_\mathrm{i} - i\lambda/d)\,, \qquad (1.3)$$

where, $k_0 = 2\pi/\lambda$ is the wave vector, λ is the wavelength of light in vacuum, n_c is the refractive index of cover medium (normally air), θ_i the incident angle and d is the grating period. At resonance, the reflected and transmitted waves consist of two coherent components: the direct reflection/transmission, called the Fresnel reflection/transmission from the corrugated profile and the diffracted coupled wave of the grating [64]. An interference occurs by the combination of

these two waves that depends on the phase difference between two waves in the vicinity of the resonance regime (phase can be varied from 0 to π). If the interfering waves have same phase then there will be no transmission and all the energy will confine in reflection and this phenomenon gives a 100% reflectance peak at a certain wavelength of incoming light wave, which is defined as resonance wavelength [64–66]. The resonance wavelength relys on the optical parameters of the grating structure i.e., grating period, grating grooved height, structural linewidth and the refractive indices of materials and surroundings [67].

In this thesis work, a GMRF structure is designed by using high index titanium dioxide (TiO_2) layer over a grating structure of fused silica (SiO_2) glass. The TiO_2 layer is acting as a waveguide medium in the structure. The GMR spectral response of the waveguide grating structure is shown in Figure 1.6, with grating parameters; grating period d = 316 nm, grating grooved height h_g = 120 nm, structural line width w = 205 nm, incident angle of incident light θ_i = 18°, refractive index of TiO_2 n_t = 2.385, refractive index of SiO_2 n_s = 1.45, refractive index of air n_a = 1, duty cycle = 65%. A GMR effect can be clearly seen at a resonance wavelength of 632.8 nm for a Transverse Electric (TE: electric field parallel to grating lines) polarized incicdent light in Figure 1.6.

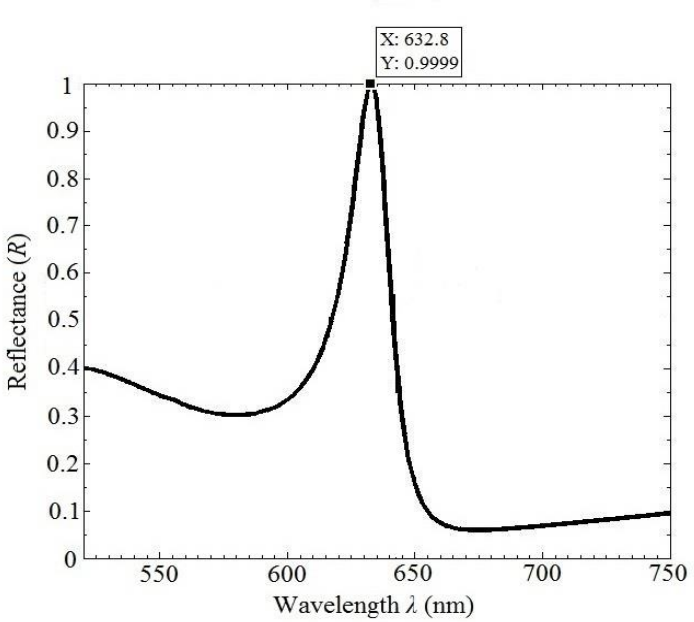

Figure 1.6: GMR effect in SiO_2 grating structure coated with TiO_2 layer of thickness t = 50 nm, with design parameters; d = 316 nm, h_g = 120 nm, w = 205 nm, duty cycle = 65%, n_t = 2.385, n_a = 1, n_s = 1.45. the GMR occurs at a resonance wavelength of 632.8 nm at an incident angle of θ_i = 18°.

1.7 Applications of Guided Mode Resonance Filters (GMRFs)

The GMRFs which are basically defined as the resonant waveguide grating (RWG) structures generate a resonance effect when a diffracted wave through a dielectric grating structure is phase matched with a leaky waveguide mode at a particular wavelength and angle of incidence of the incoming light wave [68]. The guided mode resonance (GMR) phenomenon strictly depends upon the optical and geometrical parameters of the waveguide grating structure. Along with dependency on these defined parameters, the GMR effect is also very sensitive to the polarization states of the incoming light that is TE (Transverse Electric) and TM (Transverse Magnetic) [45]. The waveguide grating structure shows resonance reflectance peaks at separate positions for both TE and TM polarization states at same geometrical parameters [69]. This sensitive behavior of GMRFs to polarization state of incident light make them very suitable candidate for applications in narrow-band filters [65], polarizers [70, 71], electro-optic switches [72, 73], laser mirrors [59, 74], wideband reflectors [75, 76], tunable filters [77–79], biosensors [80, 81]. By using appropriate design parameters, a polarization-independent GMRF structure can also be designed as biochemical sensors [82] and polarization-independent filters [70]. The versatile behavior of guided mode resonance filters (GMRFs) make them suitable candidate for application in different filtering devices such as frequency selective elements [83], security devices [84], thin film light absorbers [30], photonic meta-surfaces [85], dispersive elements [86], hybrid resonant elements [87].

In this research work, we focus on GMRF applications in solar cell technology [47, 48]. To apply this concept, we designed a hybrid structure of resonant waveguide grating with silicon (Si) solar cell. Due to GMR effect a rapid increase in the optical absorption of silicon (Si) solar cell has been observed at a specific visible area of the solar spectrum. Hence, a reasonable refinement in the efficiency of a Si solar cell is observed by applying GMRFs.

1.8 An overview of efficiency improvement techniques in solar cells

The energy transformation efficiency of a solar cell depends on the maximum number of photon absorption within the solar cell material [15]. The most of the solar cell technologies today are based on pure silicon (Si) wafer solar cells, almost 90% of the market today is served with wafer based poly-crystalline and mono-crystalline Si solar cells, while the remaining 10% is served by the thin film solar cell technologies [5]. The light coming from the sun brings photons

of different energy levels, after striking over the top surface of solar cell material photons with energy greater than the band-gap energy i.e., $h\nu > E_g$ of the cell material are absorbed in the material and excite electron-hole pairs within the active region of solar cell. While, photons having energy lower than the band-gap energy i.e., $h\nu < E_g$ are not absorbed in the cell material and eventually represents a transmission loss. This limited ratio of photon absorption in single junction Si solar cells limits their theoretical efficiency up to 30% [88]. Due to this low efficiency factor and high cost of ultra-pure Si materials, the Si wafer based solar cell technologies cannot compete with the present conventional energy resources. In the past decade, technology has been developing to improve the energy transformation efficiency of solar cells to make them feasible for efficient electrical energy generation technology [5]. Solar spectrum comprises of photons of different energy levels, whereas, single junction solar cells only absorb those photons which are greater in energy than their band-gap energy level. This limitation in photon absorption limits the efficiency of single junction solar cells [89]. There are other many factors like thermalisation losses, recombination losses, and contact and junction voltage losses that affect the energy conversion efficiency of solar cells [90]. Following are few recent advances in solar cell technologies which are focusing on the economical and better efficiency solar cell concepts.

1.8.1 Multi-junction solar cells

Multi-junction solar cells are also defined as tandem solar cells and in fact is the first concept to improve the efficiency of solar cells in the broad band spectral range of solar spectrum. These solar cells are designed by stacking multiple solar cell layers in such a way that a layer of solar cell with maximum energy band gap value should be on top of the structure following by layers of solar cells with decreasing energy band gap values. In this way, a multi-junction structure of solar cells can be developed to absorb multiple photons of different energy levels. The top layer absorbed photons of higher energy value while the lower energy photons will be transmitted to lower layers with small energy band gap values. Hence, the strength of charge carriers is increased within the active region of multiple-junction solar cell and net energy conversion efficiency of the structure is ultimately improved [91]. A schematic diagram of triple-junction solar cell is shown in Figure 1.7 (a), whereas, the quantum efficiency for the structure in solar spectrum is shown in Figure 1.7 (b) [92].

The triple-junction solar cell structure is designed by using compound semiconductor materials i.e., indium gallium phosphide (GaInP) with band gap (E_g = 1.89 eV) is used as top cell layer, gallium arsenide (GaAs) with band gap (E_g = 1.42 eV) is used as middle cell layer, and germanium (Ge) with band gap (E_g = 0.42 eV) is used as bottom layer in the structure. The quantum efficiency of the triple-junction solar cell clearly shows that each solar cell layer in the structure is absorbing photons according to their band gap values. These multi-junction solar cells can be used for efficient photon absorption in wide range of solar spectrum. Whereas, a single-junction Si solar cell can only absorb photons within the wavelength range of 300 nm to 1100 nm [89]. A practical efficiency of over 39.0% has been achieved for the triple-junction solar cell made up of GaInP/GaAs/Ge [92]. However, a theoretical study about multi-junction solar cells has revealed that by increasing the number of cell layers an efficiency of 86% can be achieved for such type of solar cells [22]. This concept of multi-junction solar cells was first developed for space applications [93].

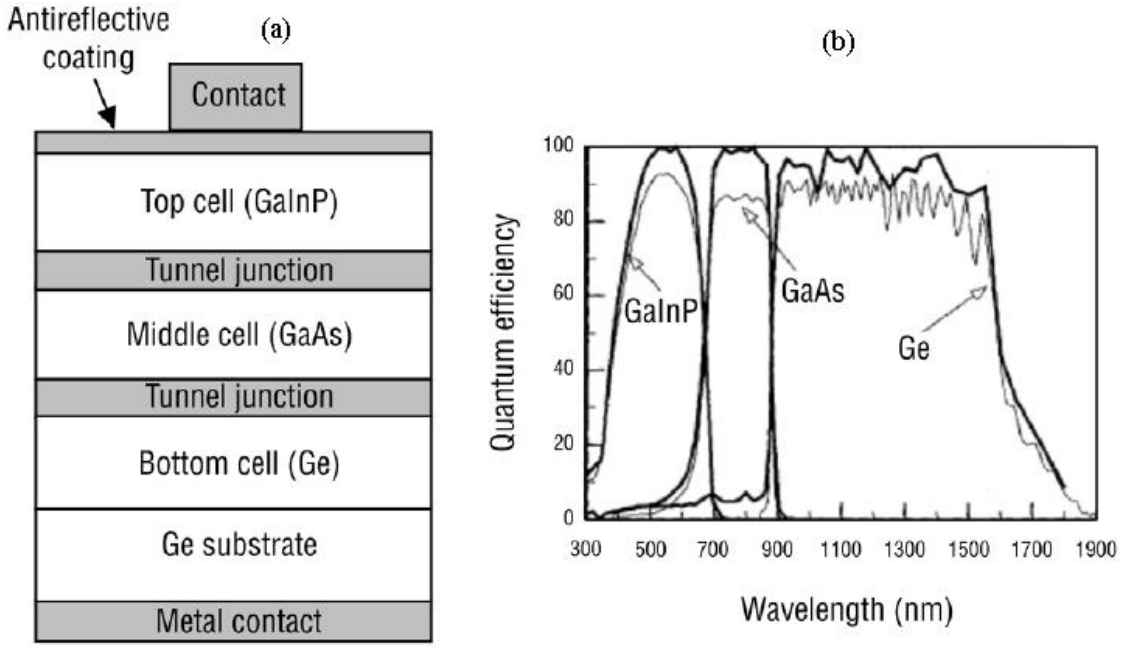

Figure 1.7: (a) A schematic diagram of triple-junction solar cell made up of GaInP/GaAs/Ge. (b) Quantum efficiency of triple-junction solar cell in wide range of solar spectrum [92].

1.8.2 Impurity photovoltaic, intermediate band and quantum well solar cells

The concept of impurity photovoltaic (IPV) solar cell elaborates an idea of modifying the host material by adding suitable impurity states within the band gap region of the respective solar cell to utilize sub-band-gap photons. In this way, multiple photons from the solar spectrum can be absorbed by the IPV solar cells and therefore improves the energy conversion efficiency [94]. Figure 1.8 (a) shows the schematic diagram of sub-band-gap photons absorption through impurity level. The major challenge in this approach is to find a wide band-gap semiconductor material which can easily merged with an efficient impurity otherwise IPV solar cells are expected to be quite efficient. Another concept which describes the formation of a narrow band gap inside the main band-gap of a solar cell material is called as intermediate band (IB) solar cell. This concept has been experimentally demonstrated by implanting Indium Arsenide (InAs) quantum dots in gallium arsenide (GaAs) semiconductor material [95]. In this way, sub-band-gap photons are absorbed by the intermediate band as shown in Figure 1.8 (b). The IPV and IB solar cells are similar in function with multi-junction solar cells as their main goal is splitting of solar spectrum to absorb multiple photons, but the usage of same material throughout and automatic interconnections between cells are prominent features in IPV and IB solar cells. The defined efficiency limit for both IPV and IB solar cells is above 63% [96, 97].

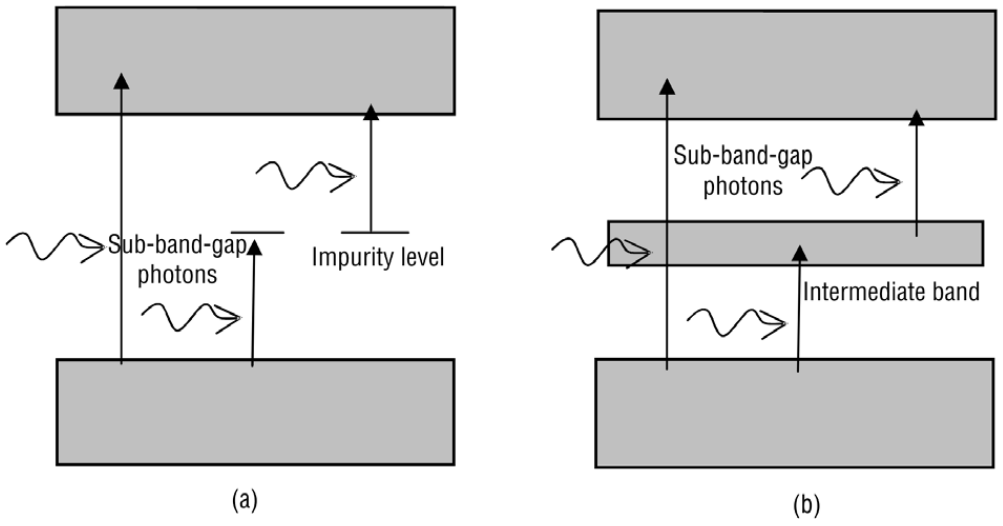

Figure 1.8: Schematic diagram of sub-band-gap photons absorption through (a) Impurity level, (b) Intermediate band-gap [94].

A multiple band-gap device having properties lying in between the properties of multi-junction and hetero-junction solar cells is called a quantum well (QW) solar cell. A device in which total current is calculated by adding the currents induced in all the materials but the voltage is defined by the lowest band-gap material is called hetero-junction solar cell. While a device in which the total voltage is calculated by adding individual voltages of all the cells but the current is calculated by the poorest of the sub-cells is called multi-junction solar cell. An efficiency improvement of 2% is indicated in a GaAsP/InGaAs (barrier/well) quantum well solar cell [98]. The improvement in efficiency is assigned to absorption edge enhancement in the quantum well solar cell. However, these modifications in solar cell concepts are still under development and need to be improved further for attaining better efficiencies.

1.8.3 Hot carrier cells

When a high-energy photon absorbed in a single junction Si solar cell it excites the electron-hole pairs and hence, increased the kinetic energy of electrons within the conduction band. These high-energy electrons are defined as hot electrons. But because of lattice scattering these hot electrons lose their kinetic energy immediately within few picoseconds. This loss of energy is called as thermalisation loss. By avoiding this loss, a prominent improvement in the efficiency of a solar cell can be achieved. In this perspective, a concept of hot carrier solar cells was developed that comprises of an absorber which sustain the energy of carriers for a long time and collect charge carriers over a restricted domain of energies, such that the extracted hot carriers are not cooled down by the cold carriers in the outer contacts [99]. The major challenge in hot carrier solar cell concept is the design of contacts. The contacts should be designed in such a way that they can easily take out hot carriers from solar cell at specific energy levels [100].

1.8.4 Absorption enhancement by spectral conversion

This concept is simplest than all the concepts presented above, a spectral conversion is a phenomenon of increasing photon absorption in solar cells by transforming very low energy photons and very high energy photons to an intermediate energy photons by using conversion layers on top and bottom of a conventional cell structure. The conversion efficiency of a simple Si solar cell for photons of energy 1.12 eV is very high, nearly 100%. Whereas, the conversion efficiency for photons of high energy value (i.e., ~3 eV) and that of low energy value (i.e., ~0.3 eV) is very low. Thus, the conversion of solar spectrum in such a way that it contains

photons of intermediate energy levels (i.e., 1.12 eV) can greatly increase the efficiency of solar cells. When two or more low-energy photons are combined to form a single high-energy photon then the process is called up-conversion. Whereas, when one high-energy photon converts into two or more low-energy photons then it is called as down-conversion. The down-conversion material should be planted on the top side of solar cell so that it can convert very higher energy photons into lower energy photons to improve the photon absorption in solar cell. While, the up-conversion material layer should be planted at the bottom side of the cell structure with reflector so that it can convert unabsorbed lower energy photons to higher energy photons and reflector reflects these converted high energy photons into the cell structure to get absorbed. Up-conversion phenomenon has been revealed by depositing NaYF4:20%Er3+ at the bottom of cell [101] and down-conversion has been revealed by depositing Si nano-crystals in a spin-on-glass matrix at the top of solar cells [102].

1.8.5 Absorption enhancement by plasmonic effects

The photon absorption on a specific wavelength can be increased by using surface Plasmon. The random movement of free electrons in the conduction band is known as Plasmon. When this random movement of conductive electrons is shifted towards the surface then it is known as surface Plasmon. When a dielectric surface coated with a metallic structure is illuminated by incident photons then it excites the surface Plasmon. The Plasmon excitation can be achieved when metallic particles are smaller in size as compared to the wavelength of incident photon. In solar cell technology surface Plasmon can increase the photon absorption by electromagnetic field enhancement [103, 104]. A layer of metal nano-particles (Ag or Au, particle sizes ranging from 20 to 100 nm) is planted on the top side of a solar cell in such a way that the surface Plasmon can be animated in the nano-particle layer. Figure 1.9 (a) shows the schematic diagram of the cell structure. The photon absorption can be increased at a specific wavelength by altering the size and formation of the nano-particles. A comparison between the photo current responses of a simple Si p-n junction diode and Si solar cell with metal nano-particles layer has been revealed by Schaadt *et al*., (see Figure 1.9 (b)) [103].

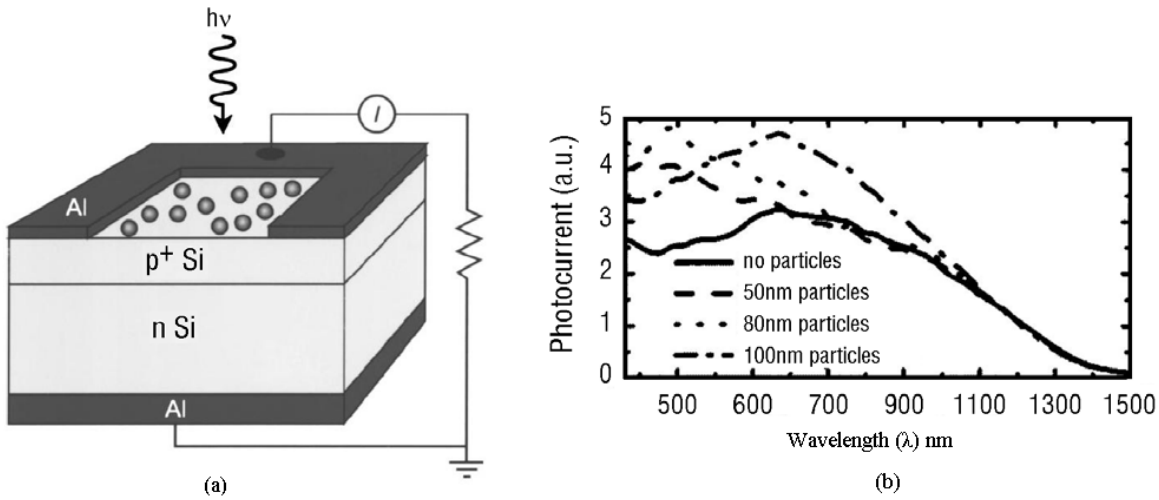

Figure 1.9: (a) Schematic view of metal nano-particles enabled Si solar cell (b) Improvement in photo-current response at Plasmon resonance wavelength for variable metal nano-particle sizes (a.u. denotes arbitrary units) [103].

1.9 Absorption enhancement in thin-film Si solar cells with photonic devices

Thin film solar cell technology is gaining interest in photovoltaic (PV) industry because of its low-cost material usage [105]. A normal wafer based Si solar cell requires a very thick material layer of almost 100 µm, while thin film Si solar cells can be easily designed with a thin material layer of thickness ranging from 250 nm to 10 µm, eventually reduces the material cost for solar cells. Due to reduction in thickness of material layer the efficiency of thin film solar cells is decreased because of the small diffusion lengths in thin films. This low efficiency element can be eliminated in thin film silicon solar cells by using effective light-trapping photonic devices, which increase the absorption of light within thin silicon layer [105, 106]. Due to recent decrease in crystalline silicon solar cells prices, the application of thin film technologies in crystalline Si solar cells are quite economical now. This section reviews the enhancement in absorption of light inside thin film Si solar cells by applying different types of ordered, disordered and hybrid photonic devices.

1.9.1 Ordered and correlated disorder photonic lattices

The efficient light confinement within the thin film crystalline Si solar cells can be achieved by using photonic crystal structures. By using appropriate design parameters, most effective light confining photonic patterns can be designed for thin film Si solar cells. Here, we review simple designs of one-dimensional (1D) binary gratings and two-dimensional (2D) square

grids of holes carved into the thin silicon film [107, 108]. An antireflection (AR) layer of transparent dielectric material and a back reflector of silver material are mounted on the top and bottom surfaces of both structures respectively. The schematic diagrams of 1D and 2D patterns in 1 μm thin silicon layer are shown in Figure 1.10 (a) and (b). The corrugated profile of the pattern enables the incoming light to propagate in different directions that are essential for integration of incident light with the partially-guided modes supported by solar cells. To explain this technique in above proposed designs proper optimization of lattice parameters: materials' fractions, etching depth and period are performed. The 2D lattice showed more short-current density J_{sc} value as compared to 1D gratings (i.e., for 2D lattice J_{sc} = 25.38 mA/cm^2 and for 1D gratings J_{sc} = 22.2 mA/cm^2) [106]. This is due to the increase in diffraction channels for 2D lattice structure, thus the light coupling phenomenon is increased within the active layer. The employment of photonic structures on solar cells is quite beneficial for light trapping, as they reduce reflection losses and increase the absorption of low energy photons within solar cells [30]. The refractive index distribution for the structures is in such a way that effective refractive index value of patterned region is in between index values of AR material and crystalline Si layer. This moderate change in indices increases the coupling of light, thus sharp resonance peaks occurs in the absorption spectra of periodic photonic structures. As the light coupling phenomenon is more in 2D lattice, thus more resonance peaks occur and eventually increases the photocurrent as compared to 1D grating. The spectral location of these resonance peaks can be changed by varying the lattice parameters. The main drawback of these perfectly ordered structures is the minimum number of diffracted waves available for light coupling phenomenon. Hence, for ordered photonic structures resonance responses are very sharp in peak but narrow in absorption cross section of each peak [106].

To improve light coupling, a concept of disorder in the lattice parameters of 1D grating structure has been introduced to increase the coupling of light [109]. A schematic diagram of a 5 μm wide super-cell with 1D grating structure is shown in the Figure 1.11. The element of disorder is introduced in the structure by changing the sizes and positions of grating's Gaussian distributions. The amount of disorder should be finite in the structure. It has been found that light harvesting in disordered structure is improved as compared to an ordered structure. The photocurrent value for an uncorrelated disordered structure is always higher as compared to a simple ordered grating structure (i.e., for disordered structure is J_{sc} = 23.4 mA/cm^2 and for

ordered structure is J_{sc} = 22.2 mA/cm^2) [106]. By further introducing the concept of correlated Gaussian disorder in the 1D grating structures it is noticed that light harvesting can be increased up to broad-band spectral range [110]. Hence, the photocurrent value for correlated disordered structure further increases up to J_{sc} = 24.32 mA/cm^2. This improvement in the value of short circuit current density for both ordered and disordered photonic structures proved that these devices can efficiently trap the incoming light and improves the absorption efficiency of thin film Si solar cells. Whereas, a flat Si solar cell only gives a short circuit current density of J_{sc} = 16.53 mA/cm^2 [111].

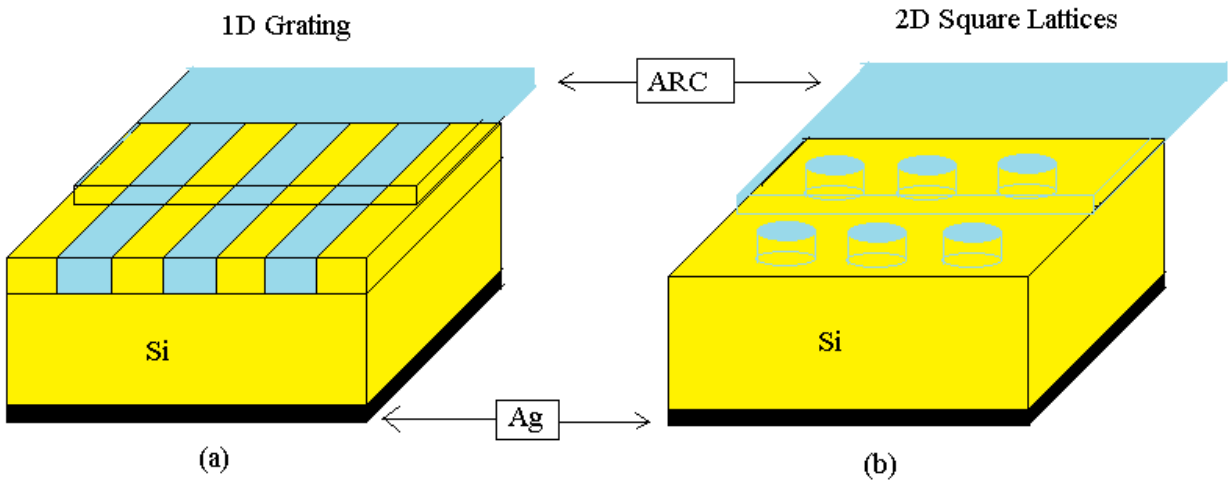

Figure 1.10: Schematic diagrams of (a) thin-film Si solar cell with 1D gratings structure (b) thin-film Si solar cell with 2D square lattices structure [106].

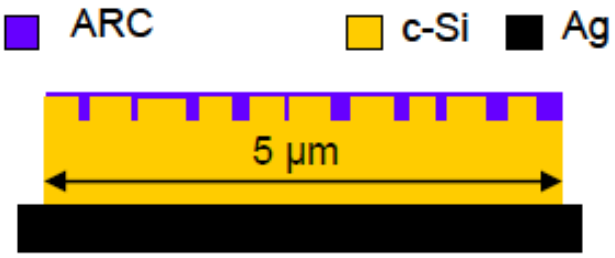

Figure 1.11: A schematic diagram of thin-film Si solar cell with disordered 1D grating structure [106].

1.9.2 Rough texture and hybrid photonic structures

Rough texture structures are another application of photonic structures for efficient light confinement in thin film Si solar cells. The concept of irregular texture surfaces is explained by surface optics [112]. Their light trapping mechanism is different from previously described light trapping techniques. Due to scattering phenomenon of light through rough texture structures; they diffuse the transmitted light. Which means that 1) photo-generation is caused by random scattering; 2) their optical parameters are independent of absorber thickness; 3) these structures are intrinsically broadband scatterers [113]. These properties make rough textures quite suitable for PV applications. Figure 1.12 (a) shows the schematic diagram for a randomly rough photonic structure mounted over a 1 µm thin Si absorber layer. The rough interfaces of the structure are designed in a thin silicon film by Gaussian Roughness, distinguished by root mean square (RMS) variation of lateral correlation length l_c and height σ. A transparent antireflection coating (ARC) and a back reflector made of silver are coated on the top surface and bottom side of the cell structure, respectively. To analyze the effect of rough textures on the solar cell efficiency short-circuit current density is calculated as a function of l_c and σ. At specific defined irregular interface parameters (l_c = 160 nm, σ = 300 nm) value of J_{sc} = 24 mA/cm^2 [106]. It can be clearly seen from the calculated value of J_{sc} that rough texture photonic structures improve the efficiency of a Si solar cell.

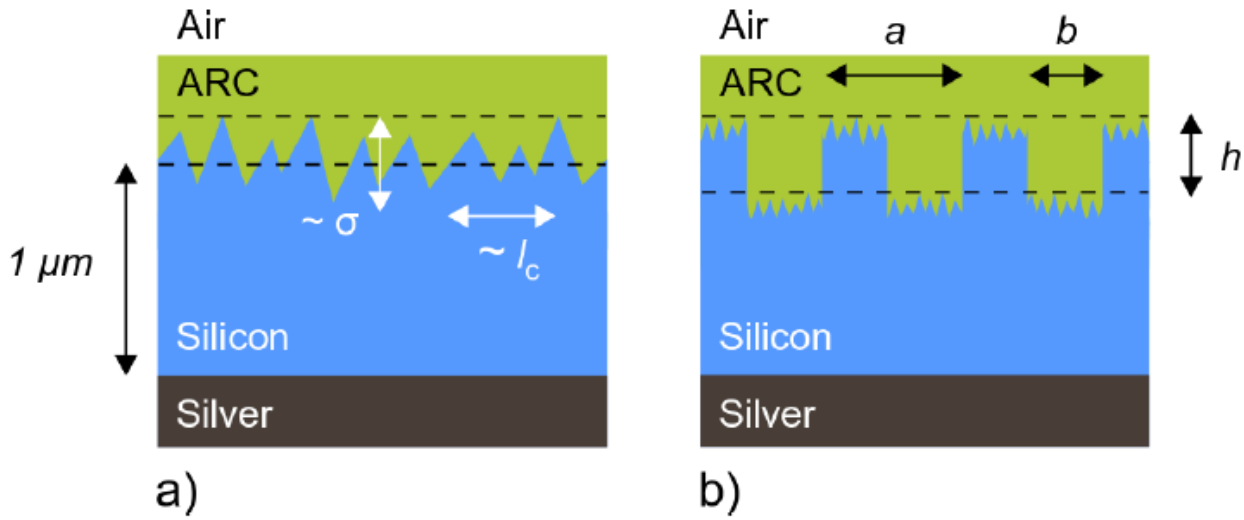

Figure 1.12: Schematic diagrams of (a) thin-film Si solar cell with rough texture photonic structure (b) thin-film Si solar cell with hybrid photonic structure [106].

Another concept that has been proposed for the efficient light confinement within the active cell layer is known as hybrid interface/hybrid photonic structure. It is in principle, a hybrid design of diffraction gratings and shallow rough interface [114, 115]. Figure 1.12 (b) demonstrates the schematic layout of the hybrid structure, the gratings are designed in a 1 μm thick Si solar cell layer with parameters: etched area width b = 180 nm, period a = 600 nm, and grating depth h = 240 nm. In this hybrid structure the parameters for rough interface are quite small as compared to optimal rough texture structures (l_c = 60 nm, σ = 80 nm). Thus, in composite structure the roughness of rough interface is reduced to a very small value as compared to rough texture surfaces. The short-circuit current density determined for the hybrid structure is J_{sc} = 23.7 mA/cm^2 which is almost equal to the J_{sc} value of rough texture structures with rough interface of 300 nm. Consequently, the hybrid structure reduces the σ to 60 nm. This reduction in σ value shows that the hybrid interface is a better technique to enhance broad-band absorption of light within thin layer Si solar cells [106].

1.9.3 GMRF photonic structures

Guided mode resonance filters (GMRFs) are resonant waveguide grating (RWG) structures which couples the incident light to leaky waveguide modes in the waveguide region to create sharp peak resonance responses. A resonance peak occurs, when a diffracted wave originated by the diffraction gratings is phase coupled with a leaky waveguide mode within the waveguide layer [45]. This guided mode resonance (GMR) effect is quite efficient in improving the absorption efficiency of a thin-layer Si solar cell. By selecting appropriate design (i.e., grating period, structure-line width, grating height, waveguide thickness, and fill factor) and optical parameters (i.e., refractive indices of structure materials and surroundings, incident angle, and wavelength of incident light), a multiple resonating GMR structure can easily be designed to increase the probability of light absorption in thin-film absorbing layers. The GMR effect elongates the photon propagation path within the active layer of Si solar cell, so that even low energy photons will get enough energy to be absorbed [66]. To demonstrate this GMR effect in thin layer Si solar cells, a grating structure of hydrogenated amorphous silicon (a-Si:H) and a waveguide layer of indium titanium oxide (ITO) coated over a glass substrate has been proposed recently [87]. Figure 1.13 (a) illustrates the schematic view of this proposed structure. A 100% resonance reflectance response and an absorbance enhancement of almost 35% for GMR enabled a-Si:H solar cell as compared to simple solar cell has been observed at a specific resonance

wavelength. With this enhancement in absorption of light, almost 40% enhancement in short-circuit current density for patterned structure has been observed as compared to planar solar cell [87].

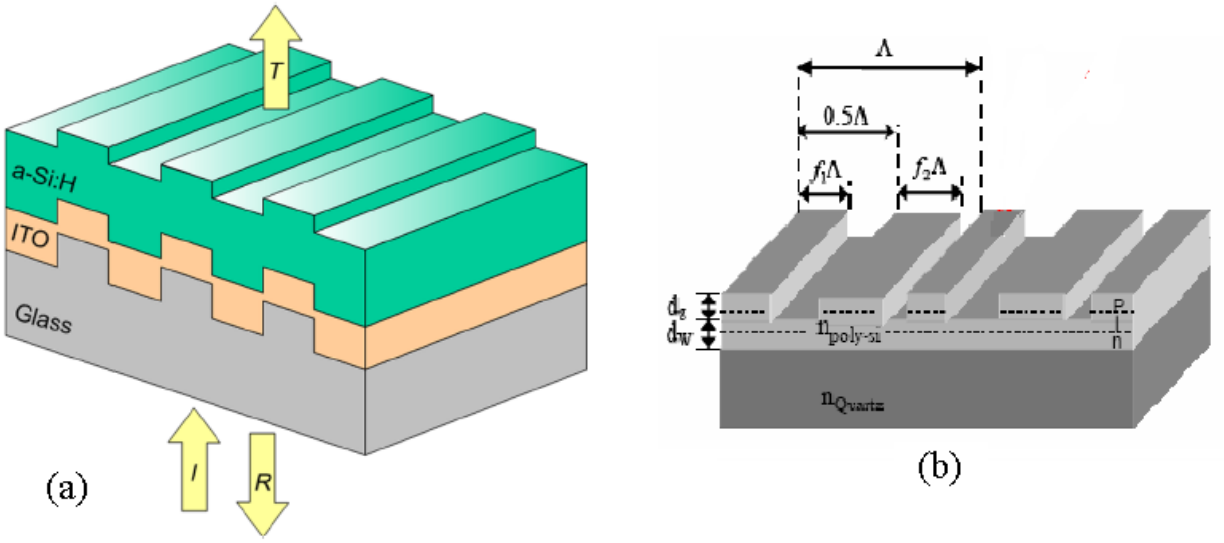

Figure 1.13: The schematic diagram of (a) GMRF enabled thin-film a-Si:H solar cell [87] (b) GMRF enabled thin film Si solar cell [116].

In another approach of designing GMR structure with thin-layer Si solar cells, a concept of introducing two filling-factor gratings has been demonstrated in GMR enabled thin-film Si solar cells [116]. Figure 1.13 (b) illustrates the schematic diagram of GMR enabled thin-layer Si solar cell with duo filling-factor gratings designed in poly-Si film placed on a quartz substrate. The concept of two filling factors f_1 and f_2 are defined in one grating period Λ of the GMR structure as shown in Figure 1.13 (b), (the sum of two fill factor is $f_1 + f_2 = 0.5$). The resonance peak occurs at a phase matching condition between diffracted waves and leaky waveguide modes in the structure, the presence of two fill factor values within a single period of gratings enabled the resonance wave to bounce several times in the active region of the solar cell [116]. Thus, eventually enhance the probability of light trapping within the Si solar cell region and hence, enhance the absorption efficiency of thin-layer Si solar cell. Through simulation results a 3-fold enhancement in absorption of light has been observed in wavelength range of 920-1040 nm for GMR enabled Si solar cell in contrast to a planar solar cell.

In the recent past many strategies have been used to upgrade the absorption efficiency of solar cells such as, diffractive optics [117, 118], antireflective layers [119, 120], plasmonics [121, 122], photonic crystals [123], guided-mode excitations [124], and 3D structures such as nano-wire [125], nano-dome [126], and nano-cone solar cells [127], but none of them is defined as the most promising light trapping technique within solar cells. The guided mode resonance filters have been recently defined as the highly sensitive and efficient light trappers which can elongates the photon propagation path in the thin absorbing layers by slow absorption of photons in broad-band solar spectrum [47, 48, 86].

1.10 Summary

Solar energy is the most vital renewable energy resource which can be utilized to produce a large amount of useful energy. We can extract three types of energies from solar energy i.e., electrical energy, thermal energy and chemical energy. The transformation of solar energy into electrical energy is gaining interest as an efficient technology for production of electricity. This chapter describes a very brief overview about solar cell technology. Solar cell is a device which when illuminated by sunlight, absorbs high energy photons and electron-hole pairs originated in the active layer of solar cell that eventually produce a potential difference at the output terminals of the device. There are many limitations in the performance of a solar cell which can limit its efficiency. The recent advances in the solar cell technology have shown that these losses or limitations can be minimized by using appropriate device structures for example, thin film solar cells, multi-junction or tandem solar cells, several electron-hole duos per photon, hot carrier cells, multiband and impurity photovoltaic cells, thermo photovoltaic and thermo photonic devices etc.

It has been found that the power transformation capability of a solar cell strongly depends upon the absorption coefficient of the incoming light within the cell material. This target can be achieved by using efficient light trapping techniques. One of the most effective light confining techniques is GMRF. This chapter summarizes the historical background of guided mode resonance phenomenon. Wood has discovered guided mode resonance (GMR) effect in his experimental work and named this concept as *Wood's Anomalies*. Later on, different researchers have contributed in this field and illustrated that these resonance effects are very sensitive and show 100% light intensity on specific resonance wavelengths. Due to these distinctive properties of GMR structures they have been proposed to use for different filtering applications in the field of optics. A GMRF is a waveguide grating structure which couples the incident light in to leaky waveguide modes and a guided mode resonance (GMR) phenomenon occurs at a specific resonance wavelength of the incoming light. GMR effect increases the probability of light absorption in solar cell due to enhancement in propagation length. Due to this enhancement in propagation length, even low energy photons get enough energy to harvest more electron-hole pairs within the active region of the cell material. This process eventually improves the operation of a silicon solar cell.

In the past decade, researchers have worked on the application of GMR effect in photovoltaics (PV). As the PV industry is growing until recently and moving towards economical and efficient solar cell concepts, the GMR devices can perform a remarkable role in the progress of PV industry. The literature showed that different techniques have been developing to upgrade the light absorption phenomenon in solar cells within a broad range of solar spectrum such as advances in solar cell concepts like quantum well solar cells, hot carrier cells, impurity photovoltaic, intermediate band gap, plasmonics, tandem solar cells, and spectral conversion layers. Similarly, photonic devices such as 1D grating structures, 2D photonic lattices, ordered and disordered 1D grating structures, randomly rough, hybrid interface, and guided mode resonance filter (GMRF) photonic structures have also proved to be an effective light confining methods for thin layer silicon (Si) solar cells. The high sensitivity and efficient light confinement phenomenon of guided mode resonance filters (GMRFs) make them a strong candidate for enhancement in light absorption of silicon (Si) solar cells.

References

[1] O. Ellabban, H. Abu-Rub, and F. Blaabjerg, "Renewable energy resources: Current status, future prospects and their enabling technology," *Renewable and Sustainable Energy Reviews*, vol. 39. pp. 748–764, 2014.

[2] B. Petroleum, "BP Statistical Review of World Energy," 2016.

[3] A. Demirbaş, "Global Renewable Energy Resources," *Energy Sources, Part A Recover. Util. Environ. Eff.*, vol. 28, no. 8, pp. 779–792, 2006.

[4] K. H. Solangi, M. R. Islam, R. Saidur, N. A. Rahim, and H. Fayaz, "A review on global solar energy policy," *Renewable and Sustainable Energy Reviews*, vol. 15, no. 4. pp. 2149–2163, 2011.

[5] International Energy Agency IEA, "Solar Photovoltaic Energy," *Technol. Roadmap*, p. 60, 2014.

[6] G. R. Timilsina, L. Kurdgelashvili, and P. A. Narbel, "Solar energy: Markets, economics and policies," *Renew. Sustain. Energy Rev.*, vol. 16, no. 1, pp. 449–465, 2012.

[7] G. K. Singh, "Solar power generation by PV (photovoltaic) technology: A review," *Energy*, vol. 53. pp. 1–13, 2013.

[8] V. Sundström, "Solar energy conversion.," *Dalton Trans.*, no. 45, p. 9951, 2009.

[9] T. Markvart and L. Castañer, "Principles of Solar Cell Operation," in *Practical Handbook of Photovoltaics*, 2012, pp. 7–31.

[10] Y. El Mghouchi, A. El Bouardi, Z. Choulli, and T. Ajzoul, "Models for obtaining the daily direct, diffuse and global solar radiations," *Renew. Sustain. Energy Rev.*, vol. 56, pp. 87–99, 2016.

[11] A. A. Lacis and J. E. Hansen, "A Parameterization for Absorption of Solar Radiation in the Earth's Atmosphere," *J. Atmos. Sci.*, vol. 31, no. 1, pp. 118–133, 1974.

[12] "Irradiation spectrum." [Online]. Available: http://www.superstrate.net/pv/illumination/spectrum.html.

[13] C. H. Henry, "Limiting efficiencies of ideal single and multiple energy gap terrestrial solar cells," *J. Appl. Phys.*, vol. 51, no. 8, pp. 4494–4500, 1980.

[14] "p-n junction of solar cell." [Online]. Available: http://www.wikiwand.com/en/P–n_junction.

[15] P. Würfel, *Physics of Solar Cells*. 2005.

[16] K. L. Chopra, P. D. Paulson, and V. Dutta, "Thin-film solar cells: an overview," *Prog. Photovoltaics Res. Appl.*, vol. 12, pp. 69–92, 2004.

[17] M. A. Green, "Third generation photovoltaics: Ultra-high conversion efficiency at low cost," *Prog. Photovoltaics Res. Appl.*, vol. 9, no. 2, pp. 123–135, 2001.

[18] W. Shockley and H. J. Queisser, "Detailed balance limit of efficiency of p-n junction solar cells," *J. Appl. Phys.*, vol. 32, no. 3, pp. 510–519, 1961.

[19] M. A. Green, K. Emery, Y. Hishikawa, and W. Warta, "Solar cell efficiency tables (version 36)," *Prog. Photovoltaics Res. Appl.*, vol. 18, no. 5, pp. 346–352, 2010.

[20] V. V. Tyagi, N. A. A. Rahim, N. A. Rahim, and J. A. L. Selvaraj, "Progress in solar PV technology: Research and achievement," *Renew. Sustain. Energy Rev.*, vol. 20, pp. 443–461, 2013.

[21] a K. O. Odziej, P. Krewniak, and S. Nowak, "Improvement in silicon thin film solar cell efficiency," *Opto-Electronics Rev.*, vol. 11, pp. 281–289, 2003.

[22] C. S. Solanki and G. Beaucarne, "Advanced solar cell concepts," *Energy Sustain. Dev.*, vol. 11, pp. 17–23, 2007.

[23] V. Sivakumar and E. Ganapathy Sundaram, “Improvement techniques of solar still efficiency: A review,” *Renew. Sustain. Energy Rev.*, vol. 28, pp. 246–264, 2013.

[24] M. R. Saleem *et al.*, “Thermal behavior of waveguide gratings” vol. 8069, p. 80690A–80690A–7, May 2011.

[25] M. Konagai, “Present status and future prospects of silicon thin-film solar cells,” *Japanese Journal of Applied Physics*, vol. 50, no. 3. 2011.

[26] G. F. Brown and J. Wu, “Third generation photovoltaics,” *Laser Photonics Rev.*, vol. 3, no. 4, pp. 394–405, 2009.

[27] W. Li, A. Furlan, K. H. Hendriks, M. M. Wienk, and R. A. J. Janssen, “Efficient tandem and triple-junction polymer solar cells,” *J. Am. Chem. Soc.*, vol. 135, no. 15, pp. 5529–5532, 2013.

[28] B. Parida, S. Iniyan, and R. Goic, “A review of solar photovoltaic technologies,” *Renewable and Sustainable Energy Reviews*, vol. 15, no. 3. pp. 1625–1636, 2011.

[29] Z.-Y. Huang *et al.*, “Spontaneous formation of light-trapping nano-structures for top-illumination organic solar cells.,” *Nanoscale*, vol. 6, pp. 2316–20, 2014.

[30] R. Dewan and D. Knipp, “Light trapping in thin-film silicon solar cells with integrated diffraction grating,” *J. Appl. Phys.*, vol. 106, no. 7, 2009.

[31] A. P. Society, “An Optical Problem , Proposed by Mr . Hopkinson , and Solved by Mr . Rittenhouse Author (s): F . Hopkinson and David Rittenhouse Source : Transactions of the American Philosophical Society , Vol . 2 (1786), pp . 201-206 Published by : American Philoso,” vol. 2, no. 1786, pp. 201–206, 2017.

[32] R. W. Wood, “On a Remarkable Case of Uneven Distribution of Light in a Diffraction Grating Spectrum,” *Proc. Phys. Soc. London*, vol. 18, no. 1, pp. 269–275, 1902.

[33] L. Rayleigh, “On the dynamical theory of gratings,” *Proc. R. Soc. London*, vol. 79, pp. 399–416, 1907.

[34] U. Fano, “The Theory of Anomalous Diffraction Gratings and of Quasi-Stationary Waves on Metallic Surfaces (Sommerfeld’s Waves),” *J. Opt. Soc. Am.*, vol. 31, no. 3, pp. 213–222, 1941.

[35] S. E. and N. B. eds D. Maystre, “Theory of Wood’d Anomalies, in Plasmonics, from basics to advanced topics,” pp. 39–83, 2012.

[36] C. H. Palmer, Jr., “Diffraction Grating Anomalies II Coarse Gratings,” *J. Opt. Soc. Am.*, vol. 46, no. 1, p. 50, 1956.

[37] a. Hessel and a. a. Oliner, “A New Theory of Wood’s Anomalies on Optical Gratings,” *Appl. Opt.*, vol. 4, no. 10, p. 1275, 1965.

[38] M. Neviere, P. Vincent, R. Petit, and M. Cadilhac, “Systematic study of resonances of holographic thin film couplers,” *Opt. Commun.*, vol. 9, no. 1, pp. 48–53, 1973.

[39] M. Neviere, R. Petit, and M. Cadilhac, “About the theory of optical grating coupler-waveguide systems,” *Opt. Commun.*, vol. 8, no. 2, pp. 113–117, 1973.

[40] L. Mashev and E. Popov, “Zero order anomaly of dielectric coated gratings,” *Opt. Commun.*, vol. 55, no. 6, pp. 377–380, 1985.

[41] H. L. Bertoni, T. Tamir, and L. H. S. Cheo, “Frequency-Selective Reflection and Transmission by a Periodic Dielectric Layer,” *IEEE Trans. Antennas Propag.*, vol. 37, no. 1, pp. 78–83, 1989.

[42] “Zero-order diffractive microstructures for security applications M.T. Gale, K. Knop and R. Morf Paul Scherrer Institute, Zurich, Switzerland,” vol. 1210, pp. 83–89, 1990.

[43] S. S. Wang, R. Magnusson, J. S. Bagby, and M. G. Moharam, “Guided-mode resonances in planar dielectric-layer diffraction gratings,” *J. Opt. Soc. Am. A*, vol. 7, no. 8, p. 1470, 1990.

[44] R. Magnusson and S. S. Wang, “New principle for optical filters,” *Appl. Phys. Lett.*, vol. 61, no. 9, pp. 1022–1024, 1992.

[45] S. S. Wang and R. Magnusson, “Theory and applications of guided-mode resonance filters.,” *Appl. Opt.*, vol. 32, no. 14, pp. 2606–2613, 1993.

[46] R. Magnusson, S. S. Wang, T. D. Black, and A. Sohn, “Resonance Properties of Dielectric Waveguide Gratings: Theory and Experiments at 4-18 Ghz,” *IEEE Trans. Antennas Propag.*, vol. 42, no. 4, pp. 567–569, 1994.

[47] S. S. Wang and R. Magnusson, “Design of waveguide-grating filters with symmetrical line shapes and low sidebands,” *Opt. Lett.*, vol. 19, no. 12, p. 919, 1994.

[48] R. Magnusson and S. S. Wang, “Transmission bandpass guided-mode resonance filters,” *Appl. Opt.*, vol. 34, no. 35, pp. 8106–9, 1995.

[49] S. Peng and G. M. Morris, “Resonant scattering from two-dimensional gratings,” *J. Opt. Soc. Am. A*, vol. 13, no. 5, p. 993, 1996.

[50] S. Peng and G. M. Morris, “Experimental demonstration of resonant anomalies in diffraction from two-dimensional gratings.,” *Opt. Lett.*, vol. 21, no. 8, pp. 549–551, 1996.

[51] D. Rosenblatt, A. Sharon, and A. a. Friesem, “Resonant grating waveguide structures,” *IEEE J. Quantum Electron.*, vol. 33, pp. 2038–2059, 1997.

[52] a. Sharon, D. Rosenblatt, and a. a. Friesem, “Resonant grating–waveguide structures for visible and near-infrared radiation,” *J. Opt. Soc. Am. A*, vol. 14, no. 11, p. 2985, 1997.

[53] S. Fan and J. Joannopoulos, “Analysis of guided resonances in photonic crystal slabs,” *Phys. Rev. B*, vol. 65, no. 23, pp. 1–8, 2002.

[54] D. Maystre, “Photonic crystal diffraction gratings.,” *Opt. Express*, vol. 8, no. 3, pp. 209–216, 2001.

[55] S. M. Loktev, N. M. Lyndin, O. Parriaux, V. A. Sychugov, and A. V Tishchenko, “Reflection of a finite light beam from a finite waveguide grating,” *Quantum Electron.*, vol. 27, no. 5, pp. 445–449, 1997.

[56] M. D. Perry *et al.*, “High-efficiency multilayer dielectric diffraction gratings.,” *Opt. Lett.*, vol. 20, no. 8, pp. 940–942, 1995.

[57] Q. He, I. Zaquine, R. André, G. Roosen, and R. Frey, “Efficient Bragg diffraction in thin semiconductor two-dimensional gratings.,” *Opt. Lett.*, vol. 33, no. 23, pp. 2868–70, 2008.

[58] M. M. J. Treacy, “Dynamical diffraction in metallic optical gratings,” *Appl. Phys. Lett.*, vol. 75, no. 5, p. 606, 1999.

[59] R. Magnusson *et al.*, “Photonic devices enabled by waveguide-mode resonance effects in periodically modulated films,” *Proc. SPIE, Nano- Micro-Optics Inf. Syst.*, vol. 5225, pp. 20–34, 2003.

[60] R. Zhao, T. Zhai, Z. Wang, and D. Liu, “Guided resonances in periodic dielectric waveguides,” *J. Light. Technol.*, vol. 27, no. 20, pp. 4544–4547, 2009.

[61] J. F. W. Turunen, “Diffractive Optics for Industrial and Commercial Applications,” *Wiley*, p. 440, 1998.

[62] M. R. Saleem, “Design , Fabrication and Analysis of Photonic Device Nanostructures Design , Fabrication and Analysis of Photonic Device Nanostructures,” 2013.

[63] S. Tibuleac and R. Magnusson, “Diffractive narrow-band transmission filters based on guided-mode resonance effects in thin-film multilayers,” *IEEE Photonics Technol. Lett.*, vol. 9, no. 4, pp. 464–466, 1997.

[64] M. R. Saleem, S. Honkanen, and J. Turunen, “Effect of substrate overetching and heat treatment of titanium oxide waveguide gratings and thin films on their optical properties,” *Appl. Opt.*, vol. 52, no. 3, pp. 422–432, 2013.

[65] S. Tibuleac and R. Magnusson, "Diffractive narrow-band transmission filters based on guided-mode resonance effects in thin-film multilayers," *IEEE Photonics Technol. Lett.*, vol. 9, pp. 464–466, 1997.

[66] M. S. Badar and M. R. Saleem, "Improved absorption efficiency of silicon (Si) solar cells through Resonant Waveguide Gratings (RWGs)-A hybrid design of RWG and Si solar cell," *Optik (Stuttg).*, vol. 128, pp. 50–56, 2017.

[67] M. R. Saleem *et al.*, "Towards athermal organic-inorganic guided mode resonance filters.," *Opt. Express*, vol. 19, no. 24, pp. 24241–51, 2011.

[68] Z. S. Liu, S. Tibuleac, D. Shin, P. P. Young, and R. Magnusson, "High-efficiency guided-mode resonance filter.," *Opt. Lett.*, vol. 23, no. 19, pp. 1556–1558, 1998.

[69] S. Tibuleac and R. Magnusson, "Reflection and transmission guided-mode resonance filters," *J. Opt. Soc. Am. A*, vol. 14, no. 7, p. 1617, 1997.

[70] Y. Ding and R. Magnusson, "Resonant leaky-mode spectral-band engineering and device applications.," *Opt. Express*, vol. 12, no. 23, pp. 5661–74, 2004.

[71] K. J. Lee *et al.*, "Silicon-layer guided-mode resonance polarizer with 40-nm bandwidth," *IEEE Photonics Technol. Lett.*, vol. 20, no. 22, pp. 1857–1859, 2008.

[72] D. F. Siriani *et al.*, "Mode control in photonic crystal vertical-cavity surface-emitting lasers and coherent arrays," *IEEE J. Sel. Top. Quantum Electron.*, vol. 15, no. 3, pp. 909–917, 2009.

[73] R. Magnusson and M. Shokooh-Saremi, "Physical basis for wideband resonant reflectors.," *Opt. Express*, vol. 16, no. 5, pp. 3456–3462, 2008.

[74] K. Iga, "Vertical-cavity surface-emitting laser: Its conception and evolution," *Jpn. J. Appl. Phys.*, vol. 47, no. 1, pp. 1–10, 2008.

[75] K. J. Lee and R. Magnusson, "Single-layer resonant high reflector in TE polarization: Theory and experiment," *IEEE Photonics J.*, vol. 3, no. 1, pp. 123–129, 2011.

[76] M. Shokooh-Saremi and R. Magnusson, "Wideband leaky-mode resonance reflectors: influence of grating profile and sublayers.," *Opt. Express*, vol. 16, no. 22, pp. 18249–18263, 2008.

[77] M. J. Uddin, T. Khaleque, and R. Magnusson, "Guided-mode resonant polarization-controlled tunable color filters," *Opt. Express*, vol. 22, no. 10, p. 12307, 2014.

[78] R. Magnusson and Y. Ding, "MEMS tunable resonant leaky mode filters," *IEEE Photonics Technol. Lett.*, vol. 18, no. 14, pp. 1479–1481, 2006.

[79] M. J. Uddin and R. Magnusson, "Guided-mode resonant thermo-optic tunable filters," *IEEE Photonics Technol. Lett.*, vol. 25, no. 15, pp. 1412–1415, 2013.

[80] V. M. N. Passaro, F. Dell'Olio, B. Casamassima, and F. De Leonardis, "Guided-Wave Optical Biosensors," *Sensors*, vol. 7, no. 4, pp. 508–536, 2007.

[81] R. Magnusson and D. Wawro, "Guided-mode resonance sensors for biochemical screening," in *Conference Proceedings - Lasers and Electro-Optics Society Annual Meeting-LEOS*, 2007, pp. 228–229.

[82] S. Kaja, "Detection of novel biomarkers for ovarian cancer with an optical nanotechnology detection system enabling label-free diagnostics," *J. Biomed. Opt.*, vol. 17, no. 8, p. 81412, 2012.

[83] B. Stiller *et al.*, "Frequency-selective excitation of guided acoustic modes in a photonic crystal fiber.," *Opt. Express*, vol. 19, no. 8, pp. 7689–94, 2011.

[84] I. R. Srimathi, M. K. Poutous, a Pung, Y. Li, R. Woodward, and E. G. Johnson, "Design and Fabrication of Mid-IR Guided Mode Resonance Filters," *Adv. Photonics Congr.*, no. c, pp. 3–5, 2012.

[85] J. a. Porto, F. J. Garcia-Vidal, and J. B. Pendry, "Transmission resonances on metallic gratings with very

narrow slits," *Phys. Rev. Lett.*, vol. 83, no. 14, pp. 2845–2848, 1999.

[86] C. Tan, J. Simonen, and T. Niemi, "Hybrid waveguide-surface plasmon polariton modes in a guided-mode resonance grating," *Opt. Commun.*, vol. 285, no. 21–22, pp. 4381–4386, 2012.

[87] T. Khaleque and R. Magnusson, "Light management through guided-mode resonances in thin-film silicon solar cells," *J. Nanophotonics*, vol. 8, no. 1, p. 83995, Mar. 2014.

[88] M. A. Green, K. Emery, Y. Hishikawa, W. Warta, and E. D. Dunlop, "Solar cell efficiency tables (version 47)," *Progress in Photovoltaics: Research and Applications*, vol. 24, no. 1. pp. 3–11, 2016.

[89] F. Meillaud, A. Shah, C. Droz, E. Vallat-Sauvain, and C. Miazza, "Efficiency limits for single-junction and tandem solar cells," *Sol. Energy Mater. Sol. Cells*, vol. 90, no. 18–19, pp. 2952–2959, 2006.

[90] M. Meral and F. Din, "Critical Factors that Affecting Efficiency of Solar Cells," *Smart Grid Renew. Energy*, vol. 1, no. 1, p. 47, 2010.

[91] K. Emery, M. Meusel, R. Beckett, F. Dimroth, A. Bett, and W. Warta, "Procedures for evaluating multijunction concentrators," in *Conference Record of the IEEE Photovoltaic Specialists Conference*, 2000, vol. 2000–Janua, pp. 1126–1130.

[92] D. J. Friedman *et al.*, "Accelerated publication 30.2% efficient GaInP/GaAs monolithic two???terminal tandem concentrator cell," *Prog. Photovoltaics Res. Appl.*, vol. 3, no. 1, pp. 47–50, 1995.

[93] R. R. King *et al.*, "Pathways to 40%-efficient concentrator photovoltaics," in *Proc. 20th European Photovoltaic Solar Energy Conference*, 2005, pp. 10–11.

[94] G. Beaucarne, A. S. Brown, M. J. Keevers, R. Corkish, and M. A. Green, "The impurity photovoltaic (IPV) effect in wide-bandgap semiconductors: An opportunity for very-high-efficiency solar cells?," *Prog. Photovoltaics Res. Appl.*, vol. 10, no. 5, pp. 345–353, 2002.

[95] A. Luque *et al.*, "Experimental analysis of the quasi-Fermi level split in quantum dot intermediate-band solar cells," *Appl. Phys. Lett.*, vol. 87, no. 8, pp. 10–13, 2005.

[96] A. S. Brown and M. A. Green, "Impurity photovoltaic effect: Fundamental energy conversion efficiency limits," *J. Appl. Phys.*, vol. 92, no. 3, pp. 1329–1336, 2002.

[97] A. Luque and A. Martí, "Increasing the Efficiency of Ideal Solar Cells by Photon Induced Transitions at Intermediate Levels," *Phys. Rev. Lett.*, vol. 78, no. 26, pp. 5014–5017, 1997.

[98] M. Mazzer *et al.*, "Progress in quantum well solar cells," *Thin Solid Films*, vol. 511–512, pp. 76–83, 2006.

[99] G. Conibeer *et al.*, "Silicon nanostructures for third generation photovoltaic solar cells," *Thin Solid Films*, vol. 511–512, pp. 654–662, 2006.

[100] C.-W. Jiang, M. a. Green, E.-C. Cho, and G. Conibeer, "Resonant tunneling through defects in an insulator: Modeling and solar cell applications," *J. Appl. Phys.*, vol. 96, no. 9, p. 5006, 2004.

[101] a. Shalav, B. S. Richards, T. Trupke, K. W. Krämer, and H. U. Güdel, "Application of NaYF[sub 4]:Er[sup 3+] up-converting phosphors for enhanced near-infrared silicon solar cell response," *Appl. Phys. Lett.*, vol. 86, no. 1, p. 13505, 2005.

[102] V. Švrček, A. Slaoui, and J. C. Muller, "Silicon nanocrystals as light converter for solar cells," in *Thin Solid Films*, 2004, vol. 451–452, pp. 384–388.

[103] D. M. Schaadt, B. Feng, and E. T. Yu, "Enhanced semiconductor optical absorption via surface plasmon excitation in metal nanoparticles," *Appl. Phys. Lett.*, vol. 86, no. 6, pp. 1–3, 2005.

[104] O. Stenzel, A. Stendal, K. Voigtsberger, and C. von Borczyskowski, "Enhancement of the photovoltaic conversion efficiency of copper phthalocyanine thin film devices by incorporation of metal clusters," *Sol. Energy Mater. Sol. Cells*, vol. 37, no. 3–4, pp. 337–348, 1995.

[105] a V Shah *et al.*, "Thin-film silicon solar cell technology," *Prog. Photovoltaics Res. Appl.*, vol. 12, no. 2–3, pp. 113–142, 2004.

[106] L. C. Andreani, A. Bozzola, P. Kowalczewski, and M. Liscidini, "Light trapping in thin-film silicon solar cells with photonic structures," in *2006 IEEE 4th World Conference on Photovoltaic Energy Conference*, 2014, vol. 4, no. 1, p. 91270M.

[107] X. Sheng, S. G. Johnson, L. Z. Broderick, J. Michel, and L. C. Kimerling, "Integrated photonic structures for light trapping in thin-film Si solar cells," *Appl. Phys. Lett.*, vol. 100, no. 11, 2012.

[108] P. Bermel, C. Luo, L. Zeng, L. C. Kimerling, and J. D. Joannopoulos, "Improving thin-film crystalline silicon solar cell efficiencies with photonic crystals," *Opt. Express*, vol. 15, no. 25, p. 16986, 2007.

[109] F. Pratesi, M. Burresi, F. Riboli, K. Vynck, and D. S. Wiersma, "Disordered photonic structures for light harvesting in solar cells," *Opt. Express*, vol. 21, no. S3, p. A460, 2013.

[110] U. W. Paetzold *et al.*, "Disorder improves nanophotonic light trapping in thin-film solar cells," *Appl. Phys. Lett.*, vol. 104, no. 13, 2014.

[111] M. Padilla, B. Michl, B. Thaidigsmann, W. Warta, and M. C. Schubert, "Short-circuit current density mapping for solar cells," *Sol. Energy Mater. Sol. Cells*, vol. 120, no. PART A, pp. 282–288, 2014.

[112] L. Forbes, "Texturing, reflectivity, diffuse scattering and light trapping in silicon solar cells," *Sol. Energy*, vol. 86, no. 1, pp. 319–325, 2012.

[113] I. Simonsen, "Optics of surface disordered systems," *The European Physical Journal Special Topics*, vol. 181. pp. 1–103, 2010.

[114] O. Isabella, J. Krč, and M. Zeman, "Modulated surface textures for enhanced light trapping in thin-film silicon solar cells," *Appl. Phys. Lett.*, vol. 97, no. 10, p. 101106, 2010.

[115] P. Kowalczewski, M. Liscidini, and L. C. Andreani, "Light trapping in thin-film solar cells with randomly rough and hybrid textures.," *Opt. Express*, vol. 21 Suppl 5, no. S5, pp. A808-20, 2013.

[116] Y.-C. Lee, C.-F. Huang, J.-Y. Chang, and M.-L. Wu, "Enhanced light trapping based on guided mode resonance effect for thin-film silicon solar cells with two filling-factor gratings," *Opt. Express*, vol. 16, no. 11, pp. 7969–7975, 2008.

[117] C. Heine and R. H. Morf, "Submicrometer gratings for solar energy applications.," *Appl. Opt.*, vol. 34, no. 14, pp. 2476–82, 1995.

[118] J. Michel and L. C. Kimerling, "Design of Highly Efficient Light-Trapping Structures for Thin-Film Crystalline Silicon Solar Cells," *IEEE Trans. Electron Devices*, vol. 54, no. 8, pp. 1926–1933, 2007.

[119] J. Müller, B. Rech, J. Springer, and M. Vanecek, "TCO and light trapping in silicon thin film solar cells," *Sol. Energy*, vol. 77, no. 6, pp. 917–930, 2004.

[120] Y. M. Song, J. S. Yu, and Y. T. Lee, "Antireflective submicrometer gratings on thin-film silicon solar cells for light-absorption enhancement.," *Opt. Lett.*, vol. 35, no. 3, pp. 276–278, 2010.

[121] H. A. Atwater and A. Polman, "Plasmonics for improved photovoltaic devices," *Nat. Mater.*, vol. 9, no. 10, pp. 865–865, 2010.

[122] H.-Y. Lin, Y. Kuo, C.-Y. Liao, C. C. Yang, and Y.-W. Kiang, "Surface plasmon effects in the absorption enhancements of amorphous silicon solar cells with periodical metal nanowall and nanopillar structures," *Opt. Express*, vol. 20, no. January, p. A104, 2012.

[123] J. G. Mutitu *et al.*, "Thin film solar cell design based on photonic crystal and diffractive grating structures.," *Opt. Express*, vol. 16, no. 19, pp. 15238–15248, 2008.

[124] K. Söderström, F. J. Haug, J. Escarŕ, O. Cubero, and C. Ballif, "Photocurrent increase in n-i-p thin film silicon solar cells by guided mode excitation via grating coupler," *Appl. Phys. Lett.*, vol. 96, no. 21, 2010.

[125] E. Garnett and P. Yang, “Light trapping in silicon nanowire solar cells,” *Nano Lett.*, vol. 10, no. 3, pp. 1082–1087, 2010.

[126] J. Zhu, C. M. Hsu, Z. Yu, S. Fan, and Y. Cui, “Nanodome solar cells with efficient light management and self-cleaning,” *Nano Lett.*, vol. 10, no. 6, pp. 1979–1984, 2010.

[127] J. Kim, A. J. Hong, J. W. Nah, B. Shin, F. M. Ross, and D. K. Sadana, “Three-dimensional a-Si:H solar cells on glass nanocone arrays patterned by self-assembled Sn nanospheres,” *ACS Nano*, vol. 6, no. 1, pp. 265–271, 2012.

Chapter 2

DEVICE DESIGN METHODOLOGY

This thesis work is divided in to two steps, in first step a Guided Mode Resonance Filter (GMRF) is designed by using Fourier Model Method (FMM), while in second step a hybrid design of silicon (Si) solar cell is designed with guided mode resonance filter (GMRF) in the Finite Difference Time Domain (FDTD) software. In the first step, a GMRF structure is defined by designing a binary grating structure on fused silica (SiO_2) coated with a thin layer of amorphous titanium dioxide (TiO_2) as a waveguide medium. Then in second step, this GMRF structure is employed on a silicon (Si) solar cell in the FDTD Designer. Hence, two versatile methods are used in this research work to analyze the guided mode resonance filters (GMRFs) behavior and their effect on the performance of a silicon (Si) solar cell. This chapter briefly focuses on the fundamental understanding and principles of these two methods.

2.1 Fourier Modal Method

Fourier modal method (FMM) is quite common and efficient method based on Fourier expansion [1, 2]. This method is applied to establish eigen-solutions of Maxwell's equations in a periodic or piecewise constant channel by developing the electromagnetic fields and permittivity functions into Fourier series, and afterwards applying boundary conditions to demonstrate fields within the grating by an algebraic eigen-value problem [3, 4]. A general overview of Maxwell's equations is presented in equations (2.1) [5]. In this method, the modulated region is divided into slabs and then finds solutions of Maxwell equations in each individual slab. By dividing the modulated region in slabs, forward and backward propagating fields comprising of modal fields appears in the result. These modal fields are pseudo-periodic and demonstrated in the form of $e^{\pm i\beta z}$; here β is defined as the propagation constant of a particular-mode. The eigenvalues for two different polarizations is demonstrated in the matrix form which defines a set of admitted values of β and a set of related transverse field distributions for each polarization. Boundary values are applied at each interface to combine the fields in all slabs. This demonstrates a comprehensive field within the modulated area, which is ultimately coupled with fields in the

homogeneous regions (Rayleigh expansions). Eventually, the issue is resolved in matrix form and then numerical calculations are performed to find the complex reflection and transmission amplitudes [6].

$$\nabla \times \boldsymbol{E}(\boldsymbol{r},t) = -\frac{\partial}{\partial t}\boldsymbol{B}(\boldsymbol{r},t), (Faraday's\ Law) \quad (2.1a)$$

$$\nabla \times \boldsymbol{H}(\boldsymbol{r},t) = \boldsymbol{J}(\boldsymbol{r},t) + \frac{\partial}{\partial t}\boldsymbol{D}(\boldsymbol{r},t), (Ampere's\ Law) \quad (2.1b)$$

$$\nabla . \boldsymbol{D}(\boldsymbol{r},t) = \boldsymbol{\rho}(\boldsymbol{r},t), (Gauss's\ Law) \quad (2.1c)$$

$$\nabla . \boldsymbol{B}(\boldsymbol{r},t) = 0, (Magnetic\ Guass's\ Law) \quad (2.1d)$$

here, ***E(r,t)***, ***B(r,t)***, ***H(r,t)***, ***D(r,t)***, ***J(r,t)***, and ***ρ(r,t)*** are the electric field, magnetic induction, magnetic field, electric displacement, current density, and electric charge densities, respectively. For free space charge region, where ***ρ(r,t)*** = 0, ***J(r,t)*** = 0, and magnetic field and electric displacement are described as; $\boldsymbol{B}(\boldsymbol{r},t) = \mu_0 \boldsymbol{H}(\boldsymbol{r},t)$, and $\boldsymbol{D}(\boldsymbol{r},t) = \epsilon_0 \boldsymbol{E}(\boldsymbol{r},t)$, respectively. The material media in our design is light and we assumed the propagation of light in free space charge region i.e., vacuum. Hence, the Maxwell's equations will be transformed into free space charge region by equations (2.2).

$$\nabla \times \boldsymbol{E}(\boldsymbol{r},t) = -\mu_0 \frac{\partial}{\partial t}\boldsymbol{H}(\boldsymbol{r},t), \quad (2.2a)$$

$$\nabla \times \boldsymbol{H}(\boldsymbol{r},t) = \epsilon_0 \frac{\partial}{\partial t}\boldsymbol{E}(\boldsymbol{r},t), \quad (2.2b)$$

$$\nabla . \boldsymbol{D}(\boldsymbol{r},t) = 0, \quad (2.2c)$$

$$\nabla . \boldsymbol{B}(\boldsymbol{r},t) = 0, \quad (2.2d)$$

here, μ_0 represents the relative permeability and ϵ_0 represents the relative permittivity of free space. In equations 2.2, the Eq. (2.2a) and Eq. (2.2b) shows the transformation of electric field ***E(r,t)*** into magnetic field ***H(r,t)*** and magnetic field ***H(r,t)*** into electric field ***E(r,t)***, respectively.

2.1.1 Theory of FMM

To keep steady flow of electromagnetic field components in Maxwell's equations over the whole permittivity modulated area, the fields are coupled within grating and homogeneous channel. Figure 2.1 shows the modulated area of the periodic waveguide grating

described as 0 < z < h. The field before and after the grating area is demonstrated as a superposition of plane waves. The z-invariant permittivity distribution $\hat{\varepsilon}(\mathrm{x},\mathrm{z})$ within the grating area and field components are developed in Fourier series. The complex magnitudes of transmitted and reflected fields are calculated by coupling the fields at inner and outer areas of the grating region and employing boundary conditions at the interfaces through S-matrix procedure [7, 8].

2.1.2 Rayleigh expansion and demonstration of modal fields within 1D grating

An accurate solution of Maxwell's equations in all channels should be found to demonstrate the modal field inside and outside of a 1D grating, uniform in y-direction. This solution should meet the boundary conditions within the bound area of grating 0 < z < h at each discontinuous interface as shown in Figure 2.1. Let us assume that half space channel (z < 0) and (z > h) are homogeneous, while their respective refractive indices n_{i} and n_{t} are real and permittivity distribution $\hat{\varepsilon}(\mathrm{x},\mathrm{z})$within the grating is z-invariant [9]. The electric field component E_{y} of reflected and transmitted *m*th diffracted orders with complex amplitudes r_{m} and t_{m} for an incident TE polarized plane wave is given as:

$$E_{\mathrm{iy}}(x,z) = e^{\mathrm{i}(\mathrm{k_{xo}x}+\mathrm{k_{zo}^{-}z})}, \tag{2.3}$$

$$E_{\mathrm{ry}}(x,z<0) = \sum_{m=-\infty}^{\infty} r_{\mathrm{m}} e^{\mathrm{i}(\mathrm{k_{xm}x}-\mathrm{k_{zm}^{-}z})}, \tag{2.4}$$

$$E_{\mathrm{ty}}(x,z>0) = \sum_{m=-\infty}^{\infty} t_{\mathrm{m}} e^{\mathrm{i}[\mathrm{k_{xm}x}+\mathrm{k_{zm}^{+}(z-h)}]}, \tag{2.5}$$

where, k_{z0}^{-}, k_{zm}^{-}, and k_{zm}^{+} are representing the normal components of the wave vectors of the incident plane wave. The following equations define the value of common elements of wave vectors for both reflected and transmitted diffraction orders.

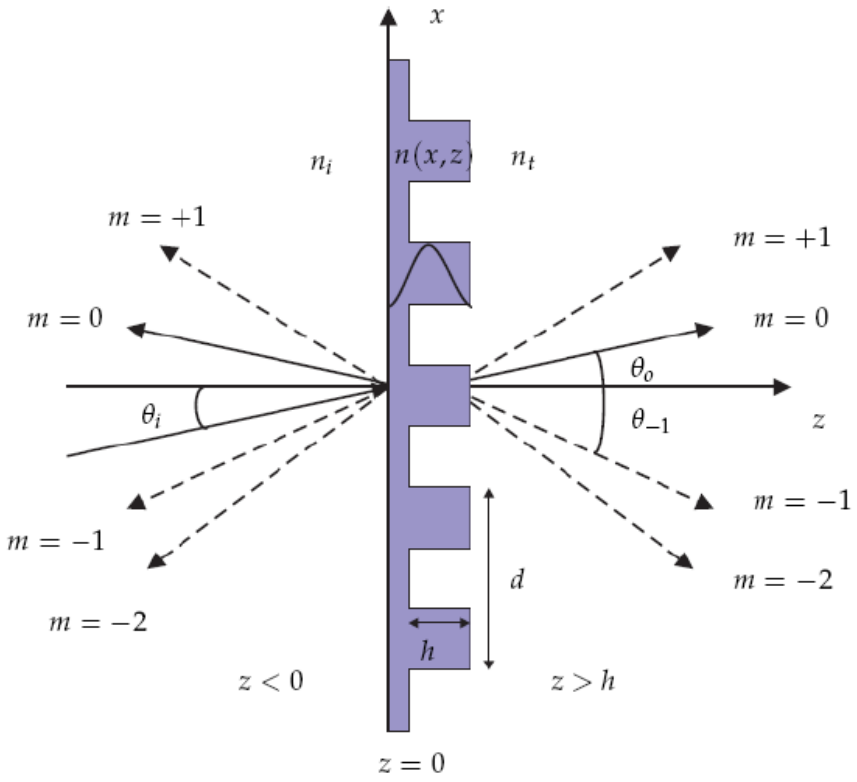

Figure 2.1: Schematic view of diffraction grating with reflected and transmitted propagating fields in different orders [10].

$$k_{zm}^{-} = \begin{cases} \sqrt{k_0^2 n_i^2 - k_{xm}^2} \;\; if \; k_{xm} \le k_0 n_i, \\ i\sqrt{k_{xm}^2 - k_0^2 n_i^2} \;\; if \; k_{xm} > k_0 n_i, \end{cases} \tag{2.6}$$

and

$$k_{zm}^{+} = \begin{cases} \sqrt{k_0^2 n_i^2 - k_{xm}^2} \;\; if \; k_{xm} \le k_0 n_t, \\ i\sqrt{k_{xm}^2 - k_0^2 n_i^2} \;\; if \; k_{xm} > k_0 n_t, \end{cases} \tag{2.7}$$

where, k_{xm} represents the tangential wave vector component, defined by grating equation $k_{xm} = k_{xo} + \frac{2\pi m}{d}$, d defines the grating period and $k_{xo} = k_o n_i \sin\theta_i$. The field within the grating structure is demonstrated as a modal expansion [9].

$$E_{gy}(x,z) = \sum_{n=-\infty}^{\infty} X_n(x)\left[a_n e^{i\beta_n z} + b_n e^{-i\beta_n (z-h)}\right], \tag{2.8}$$

where, β_n defines the modal propagation constant and a_n and b_n are anonymous modal amplitudes. The field within the grating is determined by the assessment of these anonymous modal amplitudes and $X_n(x)$ is given by,

$$X_n(x) = \sum_{m=1}^{\infty} X_{mn} e^{ik_{xm}x}. \quad (2.9)$$

2.1.3 Fourier expansion of permittivity distribution and eigenvalue equations for TE and TM modes

Assume a grating structure with period d and relative permittivity $\varepsilon_r(x)$ is distributed along x-axis. The following condition satisfied by the periodicity of $\varepsilon_r(x)$,

$$\varepsilon_r(x + d) = \varepsilon_r(x), \quad (2.10)$$

where, $\varepsilon_r(x)$is defined by Fourier series expansion as [6],

$$\varepsilon_r(x) = \sum_{t=-\infty}^{\infty} \varepsilon_t e^{i2\pi tx/d}, \quad (2.11)$$

and the Fourier coefficients are,

$$\varepsilon_t = \frac{1}{d} \int_0^d \varepsilon_r(x) e^{-i2\pi tx/d} dx. \quad (2.12)$$

The z-dependent modal solutions of Maxwell's equation which establish propagation invariant fields and x-dependent solutions that satisfy the periodicity condition are given by,

$$Z(z) = e^{\pm i\beta z}, \quad (2.13)$$

$$X(x + d) = X(x), \quad (2.14)$$

Assume the scalar component of a vector field is $U(x, z)$, which characterize the propagation mode within the grating structure of periodicity d. these fields are known as pseudo-periodic fields and are defined as [9]

$$U(x, z) = X(x) e^{ik_{xo}x} e^{i\beta z}. \quad (2.15)$$

From Eq. (2.14) the Fourier form of $X(x)$ is written as,

$$X(x) = \sum_{q=-\infty}^{\infty} X_{\mathrm{q}} e^{\mathrm{i}2\pi \mathrm{q}x/\mathrm{d}}, \tag{2.16}$$

where, the Fourier coefficient X_{q} is,

$$X_{\mathrm{q}} = \frac{1}{d}\int_{0}^{d} X(x) e^{-\mathrm{i}2\pi \mathrm{q}x/\mathrm{d}} dx. \tag{2.17}$$

Hence, Eq. (2.15) can be written as,

$$U(x,z) = \sum_{q=-\infty}^{\infty} X_{\mathrm{q}} e^{\mathrm{i}(\mathrm{k}_{\mathrm{xq}}x+\beta z)}, \tag{2.18}$$

here, $k_{\mathrm{xq}} = k_{\mathrm{xo}} + 2\pi q/d$ and the Eq. (2.18) represents the propagation invariant field $U(x, z)$ in the shape of transverse pseudo-Fourier expansion within the modulated area of the grating. Consider the Helmholtz equation with electric field (E_{y}) component to drive the eigenvalue equation for TE mode.

$$\frac{\partial^2}{\partial x^2} E_{\mathrm{y}}(x,z) + \frac{\partial^2}{\partial z^2} E_{\mathrm{y}}(x,z) + k_0^2 \varepsilon_{\mathrm{r}}(x) E_{\mathrm{y}}(x,z) = 0. \tag{2.19}$$

The E_{y} component is continuous thoroughly within the modulated region and its direction is parallel to discontinuous boundaries in *yz*-plane, while $\varepsilon_{\mathrm{r}}(x)$ is discontinuous at the boundaries. In Eq. (2.19) the term $\varepsilon_{\mathrm{r}}(x)E_{\mathrm{y}}(x, z)$ have no mutual discontinuity jumps and needs classic Laurent's rule to develop [7]:

$$\sum_{q=-\infty}^{\infty} \left[\varepsilon_{\mathrm{l-q}} - \left(\frac{k_{\mathrm{xl}}}{k_0}\right)^2 \delta_{\mathrm{lq}} \right] X_{\mathrm{q}} = (\beta/k_0)^2 X_{\mathrm{l}}. \tag{2.20}$$

Eq. (2.20) in matrix form is described as [9],

$$(\boldsymbol{E} - \boldsymbol{AIA})\boldsymbol{X} = (\beta/k_0)^2 \boldsymbol{X}. \tag{2.21}$$

Eq. (2.21) is defined as the Eigenvalue equation for TE-mode. Here, $\boldsymbol{E}$, $\boldsymbol{A}$, $\boldsymbol{I}$, and $\boldsymbol{X}$ are representing the matrices with elements $\varepsilon_{\mathrm{l-q}}$, k_{xl}/k_0, and X_{q}, respectively. Now for H_{y} component the differential equation can be written as,

$$\frac{\partial}{\partial x}\left[\varepsilon_{\mathrm{r}}^{-1}(x)\frac{\partial}{\partial x}H_{\mathrm{y}}(x,z)\right]+\frac{\partial}{\partial z}\left[\varepsilon_{\mathrm{r}}^{-1}(x)\frac{\partial}{\partial z}H_{\mathrm{y}}(x,z)\right]+k_0^2H_{\mathrm{y}}(x,z)=0, \qquad (2.22)$$

or

$$\varepsilon_{\mathrm{r}}(x)\left\{\frac{\partial}{\partial x}\left[\varepsilon_{\mathrm{r}}^{-1}(x)\frac{\partial}{\partial x}X(x)e^{\mathrm{ik_{x0}x}}\right]+k_0^2X(x)e^{\mathrm{ik_{x0}x}}\right\}=\beta^2X(x)e^{\mathrm{ik_{x0}x}}. \qquad (2.23)$$

The functions *X(x)* on the right-hand-side and $\varepsilon_{\mathrm{r}}(x)$ on the left-hand-side of Eq. (2.23) are continuous and discontinuous functions, respectively. To exercise transformed Laurent's model, the expression within curly brackets on the left-hand-side of Eq. (2.23) must be discontinuous. The Fourier series expansion for the function $\varepsilon_{\mathrm{r}}^{-1}(x)$ is given as [9],

$$\varepsilon_{\mathrm{r}}^{-1}(x)=\sum_{t=-\infty}^{\infty}\zeta_{\mathrm{t}}e^{\mathrm{i2\pi tx/d}}, \qquad (2.24)$$

with Fourier coefficients,

$$\zeta_{\mathrm{t}}=\frac{1}{d}\int_0^d\varepsilon_{\mathrm{r}}^{-1}(x)e^{-\mathrm{i2\pi tx/d}}dx. \qquad (2.25)$$

The eigenvalue equation for TM mode in matrix form is defined by affiliating inverse permittivity function $\varepsilon_{\mathrm{r}}^{-1}(x)$ to a matrix **S** with elements $\zeta_{\mathrm{l-q}}$ and employing transformed Laurent's rule with further manipulation [9].

$$\boldsymbol{S}^{-1}(\boldsymbol{I}-\boldsymbol{A}\boldsymbol{E}^{-1}\boldsymbol{A})\boldsymbol{X}=(\beta/k_0)^2\boldsymbol{X}. \qquad (2.26)$$

By utilizing excellent linear algebra algorithms and examining the suitable convergence of the series for Eqs. (2.21) and (2.26), one can easily calculate the propagation constants β_{n} and Fourier coefficients X_{qn} for both TE and TM modes, respectively. Equations (2.21) and (2.26) produce field growth in terms of modal coefficients a_{n} and b_{n} within the grating area 0 < z < h. By employing electromagnetic boundary conditions, the fields inside and outside the modulated region are coupled at boundaries z = 0 and z = h. This creates a set of immense systems of equations with anonymous modal coefficients a_{n} and b_{n}. Classical Gauss elimination method is used to solve these systems of equations for modal coefficients a_{n} and b_{n}, with this accurate solution of problem reflected and transmitted plan wave amplitudes are produced in the result.

2.2 Finite Difference Time Domain

The FDTD is dynamic, extremely meshed and user-friendly tool that permits computer assisted layout and simulation of photonic devices. This tool is established on the finite-difference time-domain (FDTD) method. The FDTD technique has been developed as a convincing engineering tool for homogeneous and diffractive optics device simulation. This software can efficiently model diffraction and scattering, polarization effects and reflection, light propagation, and dispersion and material anisotropy [11]. This method can effectively and powerfully simulate and analyze the nano/sub-micron designs with very excellent systematic properties. The designs of nano scale/sub-micron devices ensure the extreme extent of light confinement with great variation in refractive indices of materials. The FDTD software is basically consists of three main sections: the FDTD Designer, the FDTD Simulator, and the FDTD Analyzer.

2.2.1 Two-Dimensional FDTD equations

The FDTD method is established by the absolute numerical explanation of the time-dependent Maxwell's curl calculations [12]. The layout of the FDTD designer for 2D designs is defined in an *xz*-plane. The light propagates along the *z*-axis, while *y*-axis is supposed to be infinite. This supposition leads to the elimination of all *y* associated derivatives from Maxwell's equations and distribute them into two (TE and TM) discrete sets of equations.

2.2.1.1 TE waves

For 2D transverse electric (TE) polarization state, the electric component E_y and magnetic components H_x, and H_z are in non-zero state condition. So, the Maxwell's equations for these three components in a lossless media are defined as follows,

$$\frac{\partial E_y}{\partial t} = \frac{1}{\varepsilon}\left(\frac{\partial H_x}{\partial z} - \frac{\partial H_z}{\partial z}\right), \tag{2.27}$$

$$\frac{\partial H_x}{\partial t} = \frac{1}{\mu_0}\frac{\partial E_y}{\partial z}, \tag{2.28}$$

$$\frac{\partial H_z}{\partial t} = -\frac{1}{\mu_0}\frac{\partial E_y}{\partial x}, \tag{2.29}$$

where, $\varepsilon = \varepsilon_0 \varepsilon_r$ is defined as the dielectric permittivity of the material and μ_o is defined as the permeability of the free-space. The refractive index of the material is given by,

$$\eta = \sqrt{\varepsilon_r}\,. \tag{2.30}$$

All fields are assembled in a 2D order: E_y *(i, k)*, H_x *(i, k)*, and H_z *(i, k)*. Whereas, the indices *i* and *k* represents the number of space-steps along the *x* and *z*-axis, respectively. By applying the central finite-differences theorem both in space and time; the Maxwell's equations for the TE modes will be given as [13],

$$E_y^n(i,k) = E_y^{n-1}(i,k) + \frac{\Delta t}{\varepsilon \Delta z}\left[H_x^{n-\frac{1}{2}}\left(i, k+\frac{1}{2}\right) - H_x^{n-\frac{1}{2}}\left(i, k-\frac{1}{2}\right)\right] - \frac{\Delta t}{\varepsilon \Delta x}\left[H_z^{n-\frac{1}{2}}\left(i+\frac{1}{2}, k\right) - H_z^{n-\frac{1}{2}}\left(i-\frac{1}{2}, k\right)\right], \tag{2.31}$$

$$H_x^{n+\frac{1}{2}}\left(i, k+\frac{1}{2}\right) = H_x^{n-\frac{1}{2}}\left(i, k+\frac{1}{2}\right) + \frac{\Delta t}{\mu_0 \Delta z}[E_y^n(i, k+1) - E_y^n(i,k), \tag{2.32}$$

$$H_z^{n+\frac{1}{2}}\left(i+\frac{1}{2}, k\right) = H_z^{n-\frac{1}{2}}\left(i+\frac{1}{2}, k\right) - \frac{\Delta t}{\mu_0 \Delta x}[E_y^n(i+1, k) - E_y^n(i,k), \tag{2.33}$$

here, *n* represents the discrete time step, the symbols Δx is the size in real units of a space-step along the *x*-axis, Δz is the size in real units of a space-step along the *z*-axis, and Δt is the size in real units of time-step. This applied algorithm to the 2D TE waves is so-called Yee's algorithm [14]. The time-step is calculated by the Courant limit;

$$\Delta t \leq \frac{1}{c\sqrt{\frac{1}{(\Delta x)^2} + \frac{1}{(\Delta z)^2}}}, \tag{2.34}$$

where, *c* represents the speed of light.

2.2.1.2 TM waves

For 2D transverse magnetic (TM) polarization state, the electric components E_x, and E_z, and magnetic component H_y are in non-zero state condition. So, the Maxwell's equations for these three components in a lossless media are defined as follows,

$$\frac{\partial H_y}{\partial t} = -\frac{1}{\mu_0}\left(\frac{\partial E_x}{\partial z} - \frac{\partial E_z}{\partial x}\right), \tag{2.35}$$

$$\frac{\partial E_x}{\partial t} = -\frac{1}{\varepsilon}\frac{\partial H_y}{\partial z}, \tag{2.36}$$

$$\frac{\partial E_z}{\partial t} = \frac{1}{\varepsilon}\frac{\partial H_y}{\partial x}, \tag{2.37}$$

The Yee's algorithm applied in case of TE modes also explain the algorithm for TM modes in the same pattern as described in Eqs. (2.31), (2.32), and (2.33).

2.2.2 Space and time steps

The basic element of the FDTD method is the magnitude of both space and time steps. The precision, numerical dispersion and the solidity of the FDTD method are determined by space and time steps. Normally, to maintain the outcomes as correct as feasible, with minimum numerical dispersal, the mesh size better to be defined as "10 cells per wavelength", in other words, all cells should be $1/10^{th}$ or less in size than the lowest wavelength. An accurate mesh size for better simulation results can be calculated by using the following equation [15];

$$\max(\Delta x, \Delta y, \Delta z) \leq \frac{\lambda_{\min}}{10 \times \eta_{\max}}, \tag{2.38}$$

where, $\eta_{\max}$ defines the maximum refractive index value of the material. After defining the value of cell size, the maximum size for the time-steps can be calculated by using Eq. (2.34), which is defined as Courant limit.

2.2.3 FDTD simulation process

The following flow chart shows the simulation process in the FDTD software. Figure 2.2 describes the process, step by step; first a layout of a device is designed in the FDTD designer by defining all important parameters. In second step, the layout is run in the FDTD simulator and finally in the last step, all the results obtained during simulations are analyzed in the FDTD analyzer in all aspects.

2.2.4 Output Data

Algorithm of FDTD propagates the fields in time domain. Eq. (2.39) demonstrates the mathematical form of these time domain fields.

$$E(x, y, z) = A.G(x, y, z)\sin(\omega t + \phi_i), \quad (2.39)$$

where, A, G and ϕ_i denotes the field amplitude, wave profile, and phase of field, respectively. However, Eq. (2.39) does not properly define the amplitude and phase of fields. To attain proper information about amplitude/phase, stationary complex fields relative to the waveform of Eq. (2.39) are needed to define. All the important information for example, overlap integrals with modal fields, reflected and output powers, etc. are described by these complex fields and they are determined by run time Discrete Fourier Transform. The incident plane in FDTD is defined by total field/scattering field technique. The reflection function is calculated by placing observation points before the incident plane, whereas, the transmission function is calculated by placing observation points after incident plane.

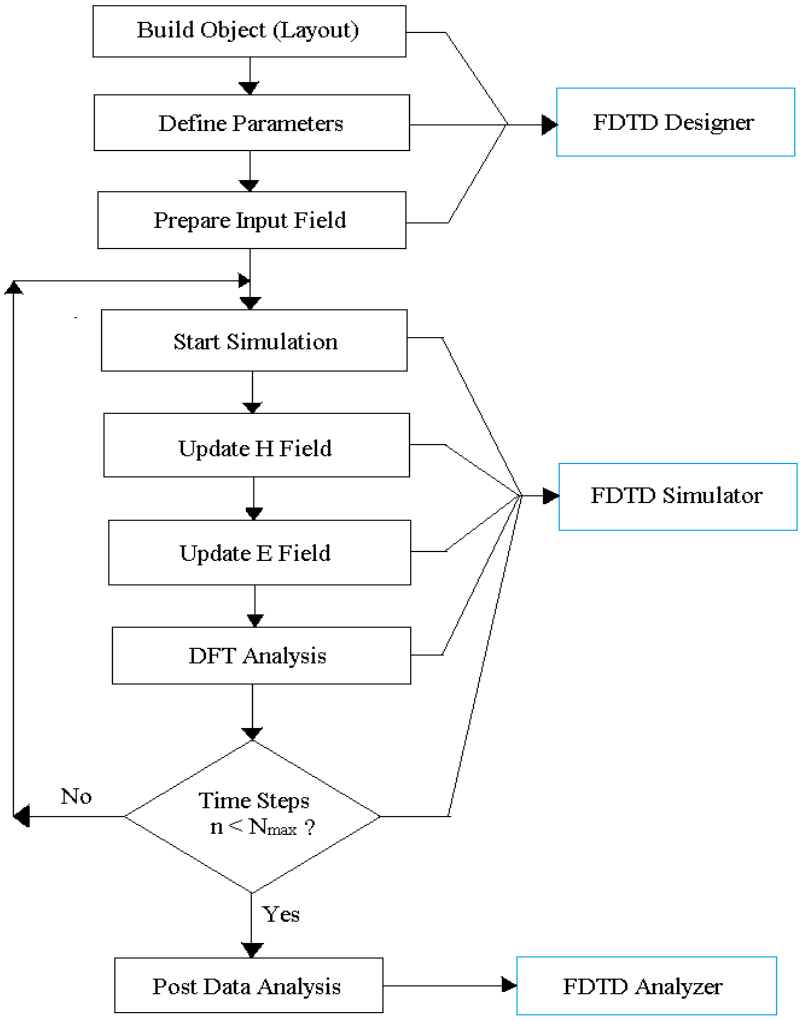

Figure 2.2: Flow chart of the FDTD simulation process.

2.3 Summary

This chapter describes all the methodological work that has been done during the research work to successfully meet the research objectives. We have used two versatile tools for successful implementation of our proposed design. The Fourier modal method (FMM) is used to design the guided mode resonance filter (GMRF), whereas, a hybrid design of integrated silicon Si solar cell with GMRF is designed by using FDTD tool. Both of these methods are quite efficient and popular tools to design photovoltaic (PV) or photonic devices. The FMM method is based on Fourier series expansion and the FDTD software is based on finite-differences theorem and Yee's algorithm.

The FMM method provides a detail analysis of GMRF structure to analyze the behavior of guided mode resonant filters (GMRFs). Successful variations in design and optical parameters of GMRF structure has been analyzed in FMM method. While, the performance of a GMRF enabled Si solar cell has been successfully analyzed in the FDTD analyzer to show the visible improvement in the optical absorption for the hybrid structure.

References

[1] M. G. Moharam, E. B. Grann, D. a. Pommet, and T. K. Gaylord, "Formulation for stable and efficient implementation of the rigorous coupled-wave analysis of binary gratings," *J. Opt. Soc. Am. A*, vol. 12, no. 5, p. 1068, 1995.

[2] M. G. Moharam, D. A. Pommet, E. B. Grann, and T. K. Gaylord, "Stable implementation of the rigorous coupled-wave analysis for surface-relief gratings: enhanced transmittance matrix approach," *J. Opt. Soc. Am. A*, vol. 12, no. 5, p. 1077, 1995.

[3] L. Li, "Use of Fourier series in the analysis of discontinuous periodic structures," *J. Opt. Soc. Am. A*, vol. 13, no. 9, p. 1870, 1996.

[4] L. Li, "New formulation of the Fourier modal method for crossed surface-relief gratings," *J. Opt. Soc. Am. A*, vol. 14, no. 10, p. 2758, 1997.

[5] J. C. Maxwell, *A Treatise on Electricity and Magnetism*. Dover, Newyork, 1954.

[6] B. L. H. Kim, J. Park, *Fourier Modal Method and its applications in Computational Nanophotonics*. CRC press, 2012.

[7] L. Li, "Formulation and comparison of two recursive matrix algorithms for modeling layered diffraction gratings," *J. Opt. Soc. Am. A*, vol. 13, no. 5, p. 1024, 1996.

[8] L. Li, "Note on the S-matrix propagation algorithm," *J. Opt. Soc. Am. A*, vol. 20, no. 4, pp. 655–660, 2003.

[9] J. F. W. Turunen, "Diffractive optics for industrial and commercial applications," Akademie Verlag, Berlin, 1997, p. 440.

[10] M. R. Saleem, "Design , Fabrication and Analysis of Photonic Device Nanostructures Design , Fabrication and Analysis of Photonic Device Nanostructures," 2013.

[11] S. D. Gedney, *Introduction to the Finite-Difference Time-Domain (FDTD) Method for Electromagnetics*, vol. 6, no. 1. 2011.

[12] S. J. Orfanidis, "Maxwell's Equations," in *Electromagnetic Waves and Antennas*, 2008, p. 18.

[13] S.-T. Chu and S. K. Chaudhuri, "A Finite-Difference Time-Domain Method for the Design and Analysis of Guided-Wave Optical Structures," *J. Light. Technol.*, vol. 7, no. 12, pp. 2033–2038, 1989.

[14] K. S. Yee, "Numerical solution of initial boundary value problems involving Maxwell's equations in isotropic media," *IEEE Trans. Antennas Propag.*, vol. 14, no. 3, pp. 302–307, 1966.

[15] M. J. Rycroft, "Computational Electrodynamics: The Finite-Difference Time-Domain Method," *Journal of Atmospheric and Terrestrial Physics*, vol. 58. pp. 1817–1818, 1996.

Chapter 3

DESIGN AND SIMULATION OF GMRFs

In this chapter, a design of Guided Mode Resonance Filter (GMRF) is demonstrated by using Fourier Modal Method (FMM). A waveguide grating structure is defined by designing a binary grating structure on fused silica (SiO_2) coated with a thin dielectric layer of titanium dioxide (TiO_2). A guided mode resonance (GMR) phenomenon of 100% efficiency is observed at appropriate design parameters of the GMRF structure under illumination. The effect of variable optical and geometrical parameters on the spectral resonance response of the GMRF structure is demonstrated by using a detailed Fourier Modal analysis. A reasonable change in the spectral position of resonance reflectance response is observed by altering the optical design parameters of the GMRF structure. The variation in optical design parameters varies the phase matching state of the waveguide grating structure and eventually alters the spectral position of guided mode resonance (GMR) response.

3.1 Guided Mode Resonant Filters (GMRFs)

Guided mode resonance filter (GMRF) comprises of a distinct high-index dielectric layer on a periodically corrugated transparent substrate to couple light [1]. The phase-matching phenomenon of the grating structure, allows the incident light to couple with a collection of waveguide modes in the waveguide layer to create multiple resonances in the GMRF structure [2]. Due to the corrugated shape of the grating structure, the generated waveguide modes are leaky with complex propagation constant [3]. A resonance phenomenon happens, when a leaky waveguide mode is phase matched with an incoming light wave at specific incident angle, wavelength and the design parameters of the grating structure [4]. This resonance phenomenon occurs at a specific resonance wavelength, which depends on the phase-matching element of the grating structure.

The GMRF structures are quite sensitive to the polarization state of the incoming light that is TE (transverse electric) or TM (transverse magnetic) [5]. Due to diffraction on the grating layer, the incident plane light waves propagate through the grating structure in different

diffracted orders, and the resonance peak arises when one of the diffracted waves couples with the waveguide mode [6]. The effective mode propagation constant β for the evanescent diffracted wave at the phase matching condition is given by equation (1.3) [7].

3.2 Design and simulation of GMRF structure

Figure 3.1 represents the schematic diagram of the GMRF structure. At first, a 1D binary grating structure is defined in a substrate of fused silica (SiO_2) with refractive index n_s, then a high index amorphous titanium dioxide (TiO_2) dielectric layer with refractive index n_t is coated on the SiO_2 grating structure. Amorphous titanium dioxide (TiO_2) material is selected as a waveguide layer due to high refractive index, high dielectric constant, high transmittance in visible and infrared regions of solar spectrum, and low scattering losses [8]. The grating structure is characterized by parameters such as height h_g, period d, and structural-line width w, so that we can define the value of fill factor by $f = w/d$. The cover medium of the GMRF structure is supposed to be air with refractive index n_a. The refractive index distribution for waveguide grating structure is defined in such a way that $n_t > n_s > n_a$. The design parameters for 1D GMRF structure are defined as: grating period d = 316 nm, refractive index of TiO_2 film n_t = 2.385, thickness of TiO_2 layer t = 50 nm, refractive index of fused silica (SiO_2) substrate n_s = 1.450, refractive index of the air n_a = 1.00, fill factor/duty cycle = 65%, structural linewidth w = 205 nm, resonance wavelength λ_r = 632.80 nm, angle of incidence θ_i = 18°, and grating grooved height h_g = 120 nm. The GMRF structure shown in Figure 3.1 is illuminated by TE-polarized incident plane light waves.

The design of sub-wavelength ($d < \lambda$) grating structure is accomplished after optimizing appropriate engineering parameters to yield 100% reflectance efficiency for TE-polarized light (electric field is parallel to grating lines) for desired resonance wavelength at a particular incident angle. The GMRF structure has been designed and analyzed in the Fourier modal method (FMM). In our design, we have analyzed the spectral reflectance response of the GMRF structure for both TE-polarized and TM-polarized light by using the FMM method. Figure 3.2(a) shows the spectral reflectance response of the GMRF structure when illuminated by a TE-polarized plane light wave at a resonance wavelength of λ_r = 632.80 nm and an incident angle of θ_i = 18°. While, Figure 3.2(b) shows the spectral reflectance response of the GMRF structure when illuminated by a TM-polarized plane light wave at a resonance wavelength of λ_r = 577.6 nm. The

full width at half maximum (FWHM) of spectral reflectance for TE-polarized light is 23.8 nm. Whereas, FWHM of spectral reflectance for TM-polarized light is just of few nm. The line-widths for resonance peaks in spectral response of guided mode resonance filters (GMRFs) are controlled by the grating modulation-amplitude and the effective mode-confinement of the GMRF structure [2]. Thus, for TM-polarized light the resonance reflectance response is highly sensitive and shows a narrow peak in the spectral response.

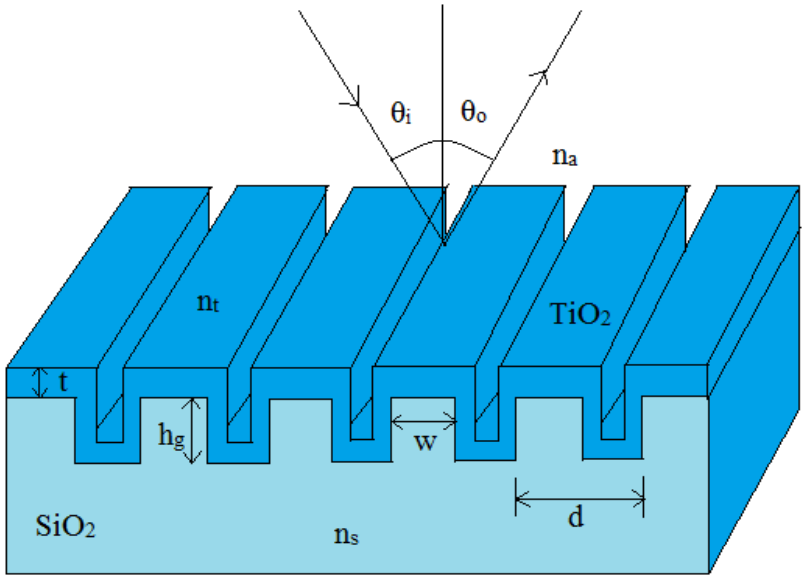

Figure 3.1: Schematic view of the guided mode resonance filter (GMRF) structure with thin amorphous TiO_2 layer coated on SiO_2 gratings [4].

The resonance wavelength λ_r of the GMRF structure strongly depends on the incident angle θ_i of the incoming light, slight variations in the incident angle can change the spectral position of the resonance wavelength in the broad-band. Figures 3.3(a) and (b) shows 2D simulation results for the variation in the spectral reflectance response of the GMRF structure by varying the angle of incidence of the incoming light for both TE- and TM-polarized incoming light waves, respectively. A gradual increase in the value of incident angle θ_i also increases the value of resonance wavelength λ_r for the spectral reflectance response of the GMRF structure. This increase in resonance wavelength is due to the change in phase matching condition of the grating structure, as depicted in equation (1.3). The effect of variation of incident angle θ_i on the resonance wavelength λ_r is also demonstrated in figures 3.4(a) and (b) for both TE- and TM-polarized incoming light waves, respectively.

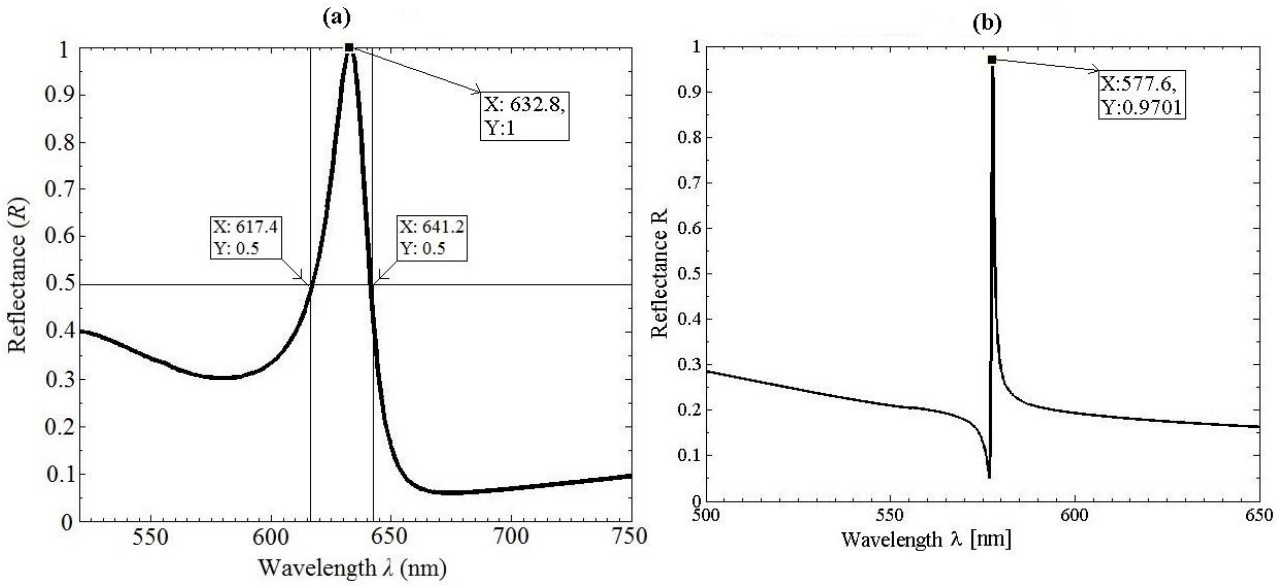

Figure 3.2: Spectral reflectance response of a GMRF structure when illuminated by (a) TE-polarized light at $\lambda_r = 632.80$ nm and (b) TM-polarized light at $\lambda_r = 577.6$ nm.

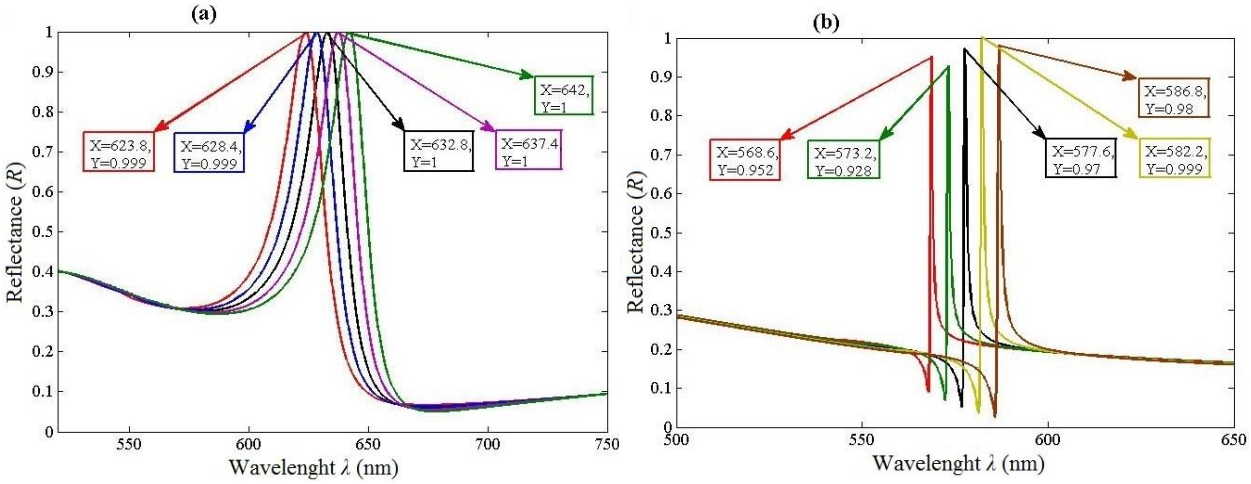

Figure 3.3: 2D simulation results for effect of variation in incident angle θ_i of incoming light on the resonance wavelength λ_r of the GMRF structure (a) for TE-polarized light (b) for TM-polarized light.

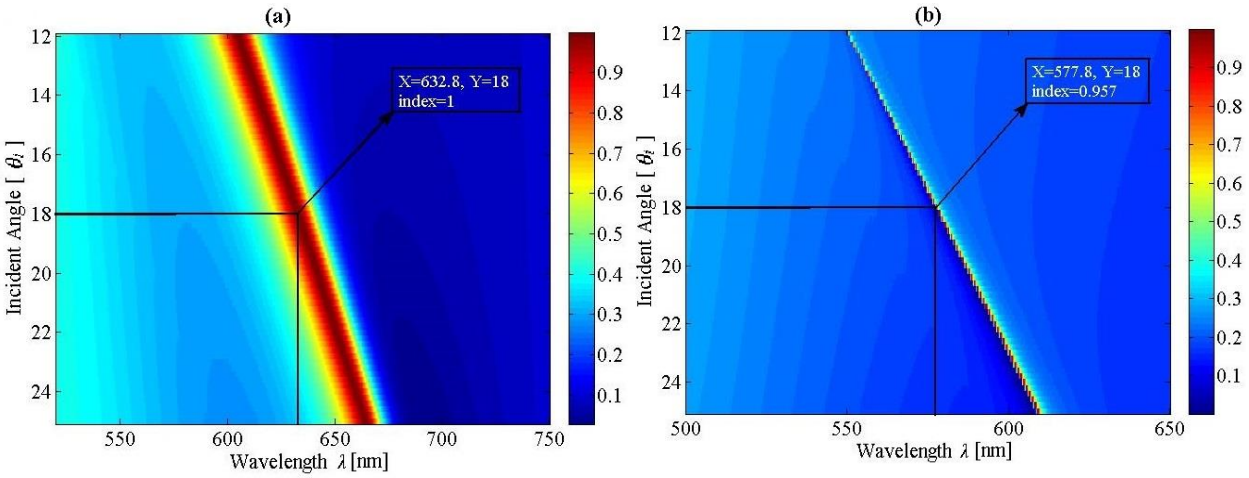

Figure 3.4: 3D simulation results for effect of variation in incident angle θ_i of incoming light on the resonance wavelength λ_r of the GMRF structure (a) for TE-polarized light (b) for TM-polarized light.

3.2.1 Effect of variable parameters on spectral reflectance response of GMRF structure

The appropriate selection of the design parameters of GMRF structure is quite important in defining the locations of spectral resonance responses in the broad-band wavelength range. A guided-mode resonance (GMR) phenomenon with 100% reflectance can be achieved by optimizing the design parameters d, f, h_g, n_t, n_s, and θ_i. In our design, we have analyzed the effect of variation in design parameters on the spectral reflectance response of GMRF structure by using the FMM method. The proposed value of d in our design is d = 316 nm, but to analyze the grating behavior at different grating period values we have varied the value of d from 312 nm to 320 nm and observed the spectral reflectance response of GMRF structure at variable design parameters. Figure 3.5, shows the effect of variation in grating grooved height h_g and fill factor f on the spectral reflectance response of the GMRF structure at different grating period d values. This implies that with the gradual increase in the value of d the GMR spectral response for the GMRF structure is shifting towards the lower values of f and h_g, as illustrated in Figures 3.5(a) to (i). At the proposed value of grating period in our design i.e., d = 316 nm, Figure 3.5(e) indicates that an increase in the value of grating grooved height h_g can be compensated by decreasing the fill factor f to attain resonance peak at accurate spectral position. The index 1 on the palette within in the figures represents 100% intensity of light. Table 3.1, represents the variation in the

values of fill factor f and grating height h_g with respect to variation in values of grating period d for GMRF structure in the tabulated form.

Figure 3.6, depicts the probability of excellent tuning of the resonance wavelength by varying the incident angle of the input light. The effect on spectral reflectance response of the GMRF structure by varying resonance wavelength and incident angle has been analyzed at different grating period values i.e., d = 312 nm to 320 nm. This implies that the resonance wavelength λ_r for GMR spectral response increases with the value of d and incident angle θ_i of the incoming light waves, as illustrated in Figures 3.6(a) to (i). The change in incident angle θ_i changes the diffracted angle θ_m of the evanescent diffracted waves, which in turn changes the phase matching condition for the leaky waveguide modes and diffracted waves, and eventually, will change the spectral position of the resonance peak at a particular resonance wavelength. The index 1 on the palette in the figures indicates the 100% intensity of light. Table 3.2, represents the variation in resonance wavelength λ_r with respect to variation in values of grating period d for GMRF structure in the tabulated form. Figure 3.7, demonstrates the effect of variation in the refractive indices of waveguide layer TiO_2 and grating layer SiO_2 on the spectral reflectance response of the GMRF structure at different values of grating period i.e., d = 312 nm to 320 nm. This implies that an increase in the value of grating period shifts the GMR spectral response towards the lower values of refractive indices of SiO_2 and TiO_2 materials, as illustrated in Figures 3.7(a) to (i). Whereas, the simulation results in Figure 3.7 represents a tolerance of refractive indices of these two materials for peak resonance. The index 1 on the palette in the figures indicates the 100% intensity of light.

All the simulation results shown below in the Figures 3.5, 3.6 and 3.7, illustrated that a change in the spectral position of the specular reflectance of the GMRF structure has been observed at variable design parameters. The reason for this change is that variable design parameters will alter the leaky waveguide modes generated through the GMRF structure and subsequently alter the resonance peak positions and the coupling power between the incoming light and leaky waveguide [9].

Table 3.1: Effect of variation of grating period *d* values on design parameters: fill factor *f* and grating height h_g of GMRF structure.

Grating Period (*d*) (nm)	**Fill Factor (*f*)**	**Grating Height (h_g) (nm)**	**Intensity of Light (%)**
312	0.68	125	86.7
313	0.68	125	94.9
314	0.68	125	99.3
315	0.673	123	100
316	**0.65**	**120**	**100**
317	0.635	116	99
318	0.632	115.3	94.5
319	0.631	115.2	87.2
320	0.634	115	79.1

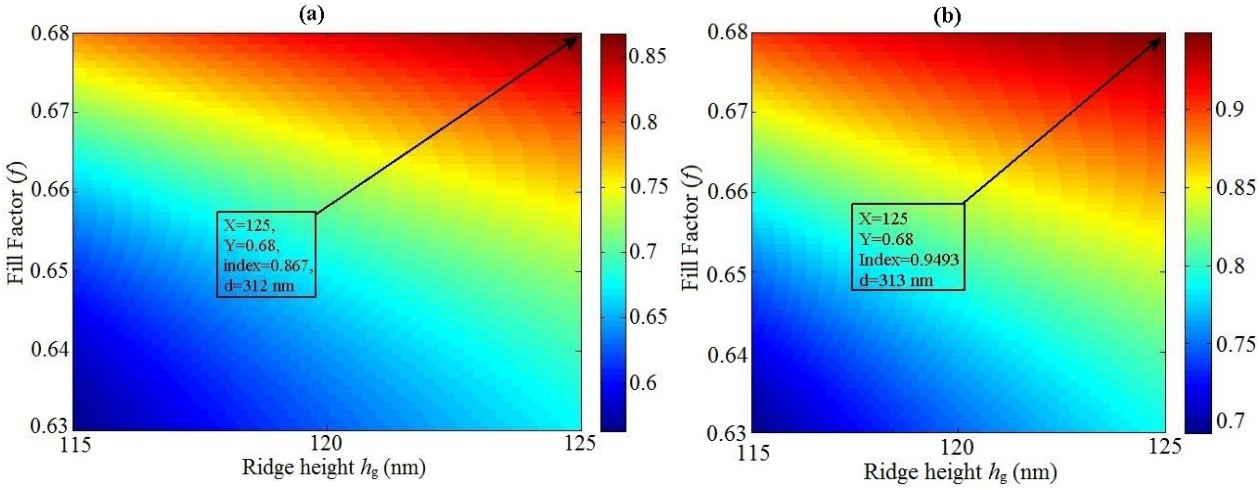

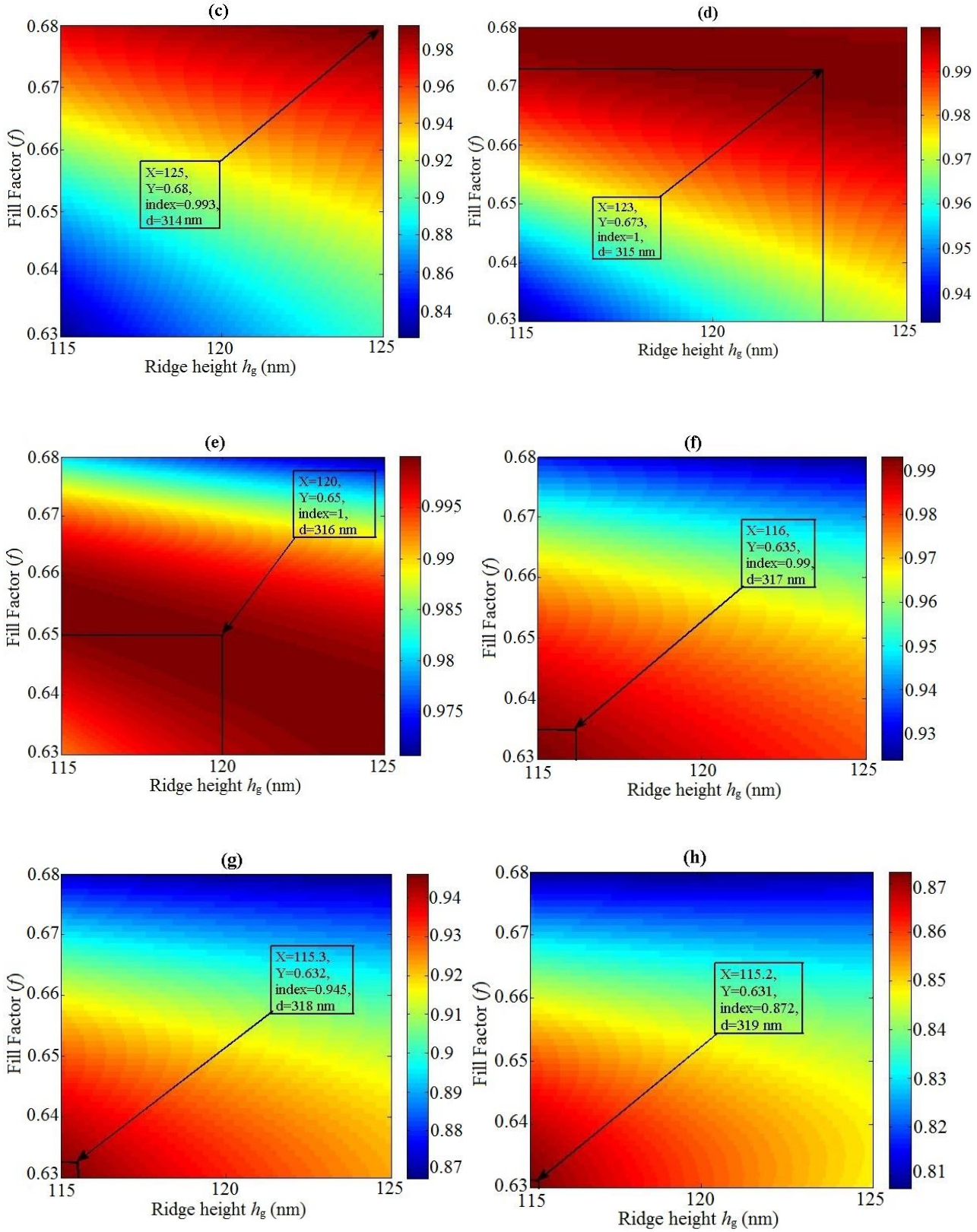
(c)
X=125,
Y=0.68,
index=0.993,
d=314 nm
Fill Factor (f)
Ridge height h_g (nm)
(d)
X=123,
Y=0.673,
index=1,
d= 315 nm
Fill Factor (f)
Ridge height h_g (nm)
(e)
X=120,
Y=0.65,
index=1,
d=316 nm
Fill Factor (f)
Ridge height h_g (nm)
(f)
X=116,
Y=0.635,
index=0.99,
d=317 nm
Fill Factor (f)
Ridge height h_g (nm)
(g)
X=115.3,
Y=0.632,
index=0.945,
d=318 nm
Fill Factor (f)
Ridge height h_g (nm)
(h)
X=115.2,
Y=0.631,
index=0.872,
d=319 nm
Fill Factor (f)
Ridge height h_g (nm)

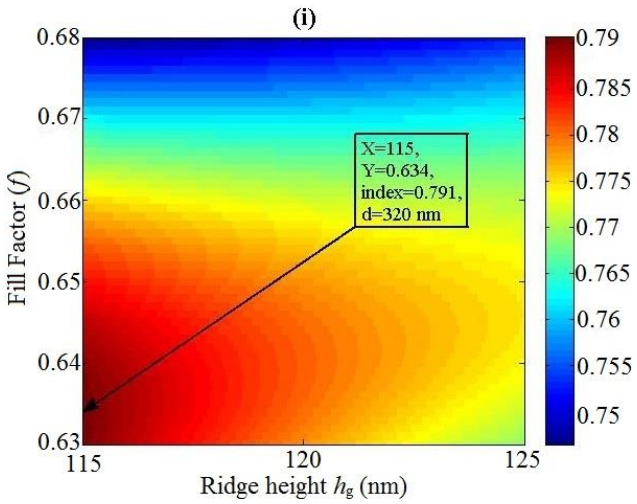

Figure 3.5: Effect of variations in design parameters of fill factor *f* and grating height h_g on the spectral reflectance response of the RWG structure; (a) at *d* = 312 nm, (b) at *d* = 313 nm, (c) at *d* = 314 nm, (d) at *d* = 315 nm, (e) at *d* = 316 nm, (f) at *d* = 317 nm, (g) at *d* = 318 nm, (h) at *d* = 319 nm, (i) at *d* = 320 nm, respectively.

Table 3.2: Effect of variation of grating period *d* values on resonance wavelength λ_r of GMRF structure.

Grating Period (*d*) (nm)	**Resonance Wavelength (λ_r) (nm)**	**Intensity of Light (%)**
312	627	99.8
313	628	99.9
314	630	99.9
315	631	99.8
316	**632.8**	**100**
317	635	99.8
318	636	99.9
319	638	99.9
320	639	99.9

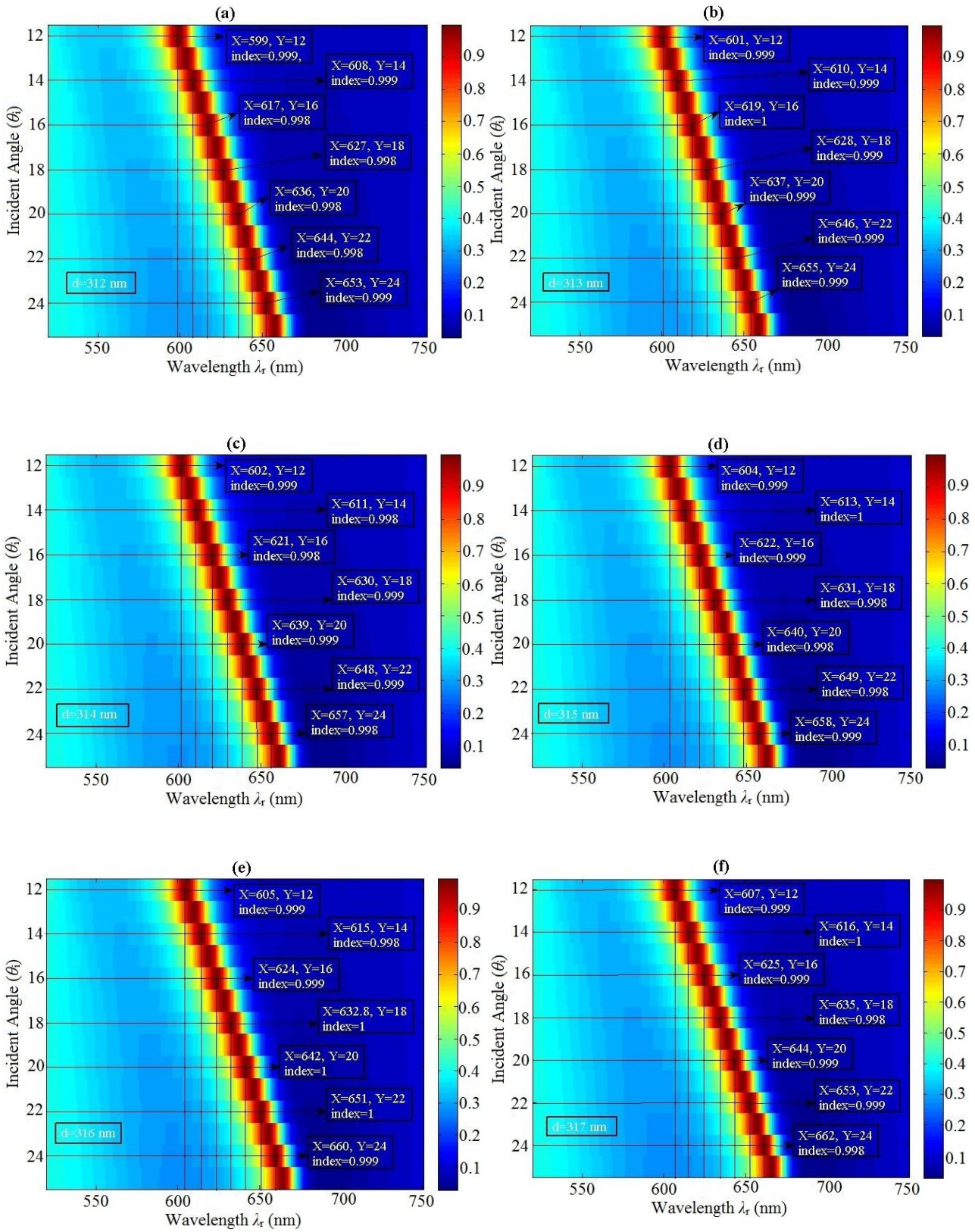
(a)
X=599, Y=12
index=0.999,
X=608, Y=14
index=0.999
X=617, Y=16
index=0.998
X=627, Y=18
index=0.998
X=636, Y=20
index=0.998
X=644, Y=22
index=0.998
X=653, Y=24
index=0.999
d=312 nm
(b)
X=601, Y=12
index=0.999
X=610, Y=14
index=0.999
X=619, Y=16
index=1
X=628, Y=18
index=0.999
X=637, Y=20
index=0.999
X=646, Y=22
index=0.999
X=655, Y=24
index=0.999
d=313 nm
(c)
X=602, Y=12
index=0.999
X=611, Y=14
index=0.998
X=621, Y=16
index=0.998
X=630, Y=18
index=0.999
X=639, Y=20
index=0.999
X=648, Y=22
index=0.999
X=657, Y=24
index=0.998
d=314 nm
(d)
X=604, Y=12
index=0.999
X=613, Y=14
index=1
X=622, Y=16
index=0.999
X=631, Y=18
index=0.998
X=640, Y=20
index=0.998
X=649, Y=22
index=0.998
X=658, Y=24
index=0.999
d=315 nm
(e)
X=605, Y=12
index=0.999
X=615, Y=14
index=0.998
X=624, Y=16
index=0.999
X=632.8, Y=18
index=1
X=642, Y=20
index=1
X=651, Y=22
index=1
X=660, Y=24
index=0.999
d=316 nm
(f)
X=607, Y=12
index=0.999
X=616, Y=14
index=1
X=625, Y=16
index=0.999
X=635, Y=18
index=0.998
X=644, Y=20
index=0.999
X=653, Y=22
index=0.999
X=662, Y=24
index=0.998
d=317 nm
Incident Angle (θ_i)
Wavelength λ_r (nm)

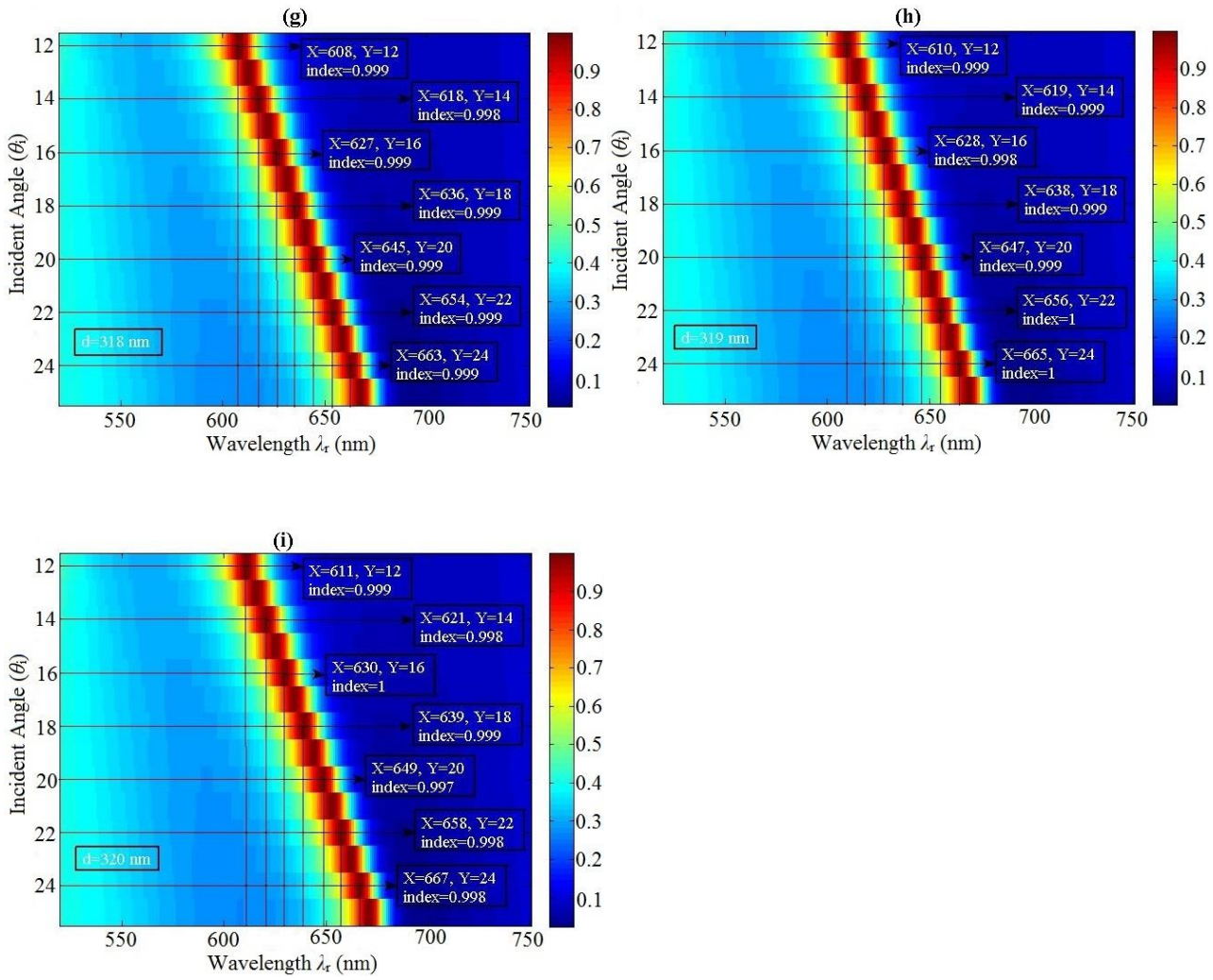

Figure 3.6: Effect of variations in design parameters of incident angle θ_i and resonance wavelength λ_r on the spectral reflectance response of the RWG structure; (a) at d = 312 nm, (b) at d = 313 nm, (c) at d = 314 nm, (d) at d = 315 nm, (e) at d = 316 nm, (f) at d = 317 nm, (g) at d = 318 nm, (h) at d = 319 nm, (i) at d = 320 nm, respectively.

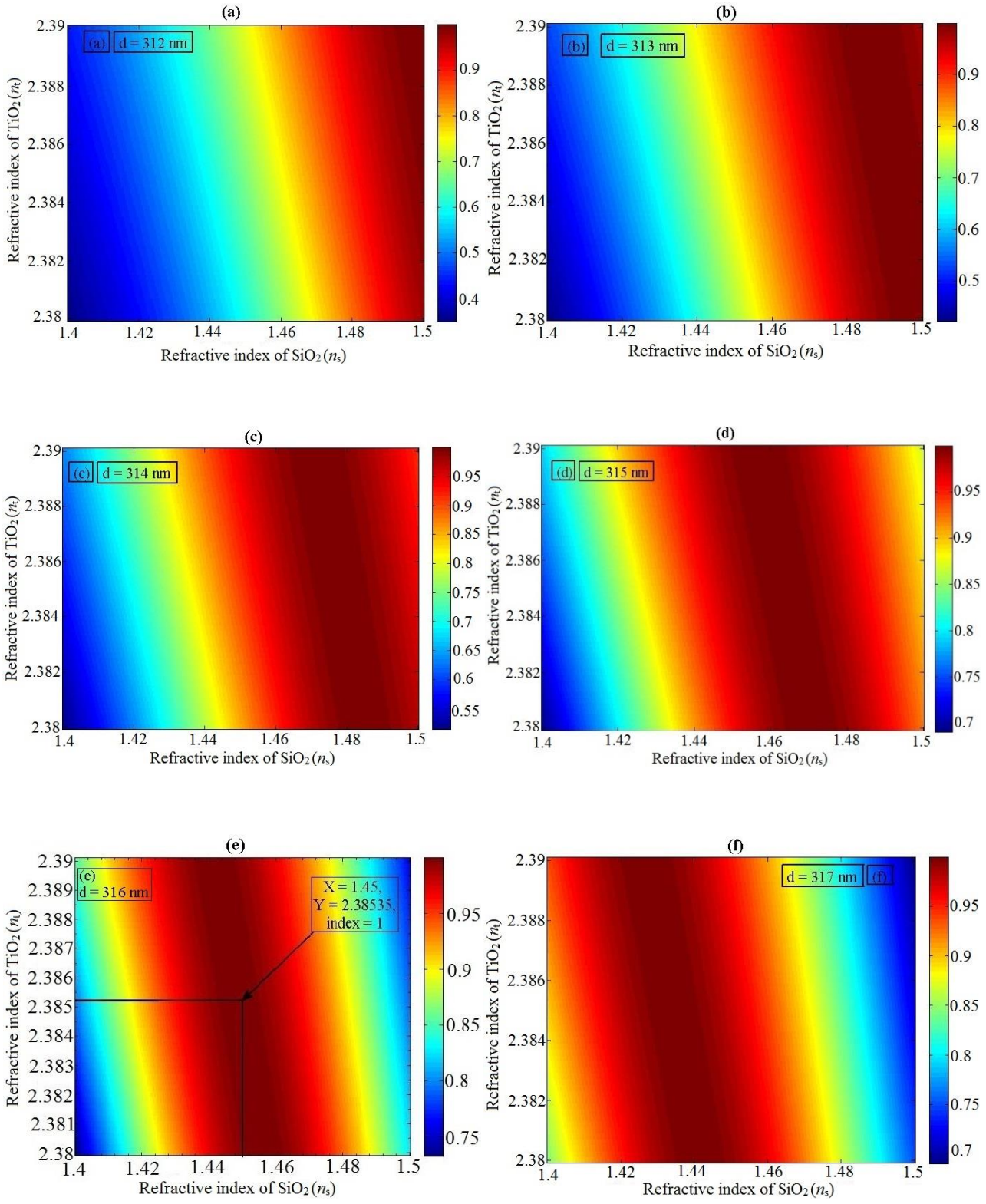
(a)
(a) d = 312 nm
(b)
(b) d = 313 nm
(c)
(c) d = 314 nm
(d)
(d) d = 315 nm
(e)
(e) d = 316 nm
X = 1.45, Y = 2.38535, index = 1
(f)
d = 317 nm (f)
Refractive index of TiO2 (nt)
Refractive index of SiO2 (ns)

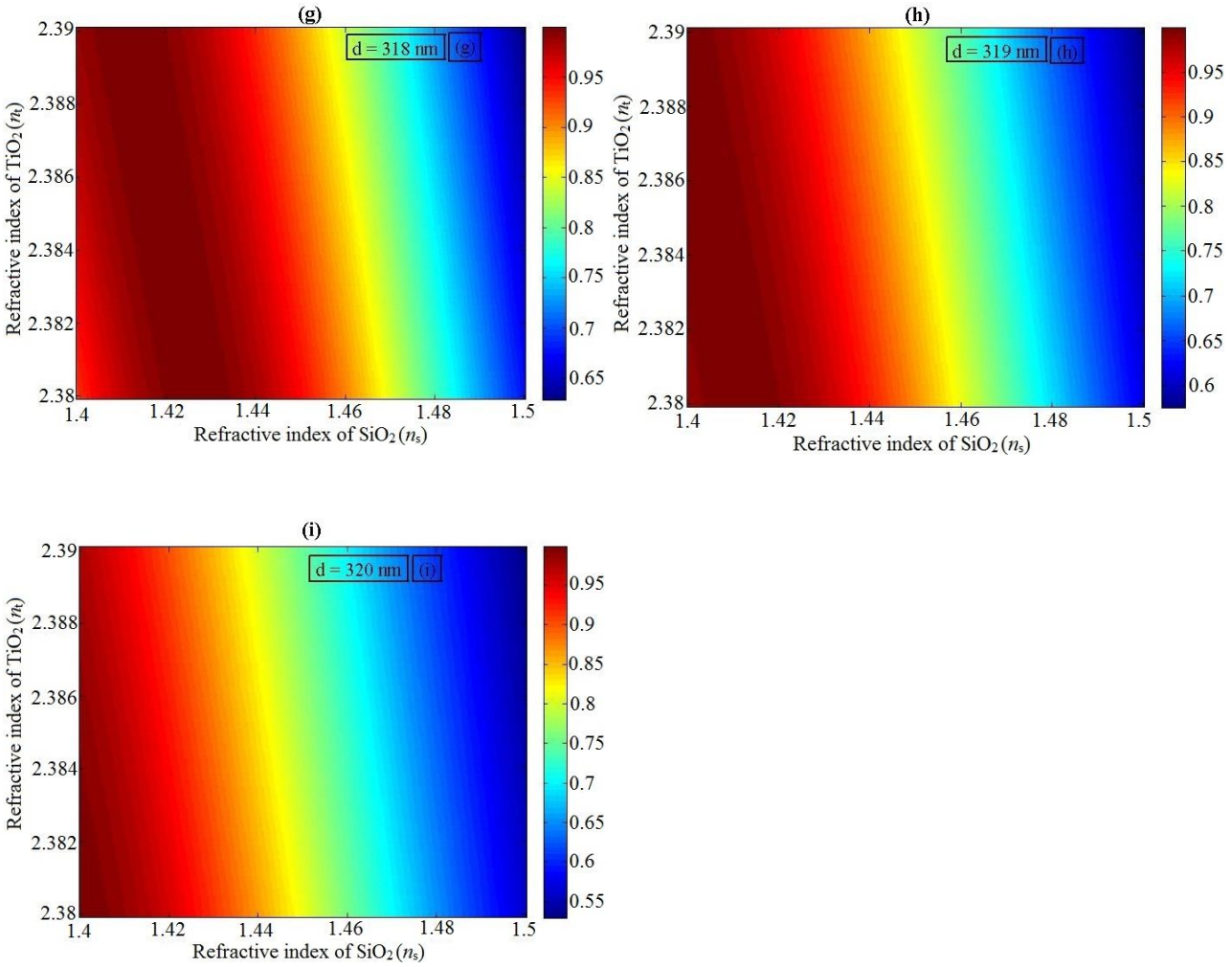

Figure 3.7: Effect of variations in design parameters of refractive indices of SiO_2 n_s and TiO_2 n_t on the spectral reflectance response of the RWG structure; (a) at d = 312 nm, (b) at d = 313 nm, (c) at d = 314 nm, (d) at d = 315 nm, (e) at d = 316 nm, (f) at d = 317 nm, (g) at d = 318 nm, (h) at d = 319 nm, (i) at d = 320 nm, respectively.

3.3 Summary

In this chapter design and simulation results of guided mode resonance filter (GMRF) is presented in detail. The GMRF structure is defined by designing a grating structure in a fused silica (SiO_2) substrate coated with a thin high index dielectric amorphous titanium dioxide (TiO_2) layer. The TiO_2 layer is acting as a waveguide medium in the structure. At appropriate design parameters, a resonance reflectance response with 100% efficiency is obtained from the design of guided mode resonance filter (GMRF) structure by using the Fourier modal method (FMM). A guided mode resonance (GMR) response happens when an incoming light wave is combined with the leaky waveguide mode within the waveguide layer. By using the FMM method, a detailed analysis of the effect of variations in design parameters on the spectral reflectance response of the GMRF structure is demonstrated. The simulation results of the GMRF structure at variable parameters have demonstrated a reasonable change in the resonance locations of the waveguide grating structure. The variable design parameters affect the phase matching condition of the grating element, thus, vary the leaky waveguide mode generated by the GMRF structure and alter the resonance peak positions and the coupling power between the waveguide modes and the incoming light waves. Through a detail FMM analysis the resonant behavior of the guided mode resonance filter (GMRF) has been observed over variable design parameters and calculated a 100% resonance reflectance response at a particular resonance wavelength.

References

[1] J. M. Bendickson, E. N. Glytsis, T. K. Gaylord, and D. L. Brundrett, "Guided-mode resonant subwavelength gratings: effects of finite beams and finite gratings.," *J. Opt. Soc. Am. A. Opt. Image Sci. Vis.*, vol. 18, no. 8, pp. 1912–1928, 2001.

[2] S. S. Wang and R. Magnusson, "Theory and applications of guided-mode resonance filters.," *Appl. Opt.*, vol. 32, no. 14, pp. 2606–2613, 1993.

[3] T. Khaleque and R. Magnusson, "Light management through guided-mode resonances in thin-film silicon solar cells," *J. Nanophotonics*, vol. 8, no. 1, p. 83995, Mar. 2014.

[4] M. S. Badar and M. R. Saleem, "Improved absorption efficiency of silicon (Si) solar cells through Resonant Waveguide Gratings (RWGs) ??? A hybrid design of RWG and Si solar cell," *Optik (Stuttg).*, vol. 128, pp. 50–56, 2017.

[5] D. Rosenblatt, A. Sharon, and A. a. Friesem, "Resonant grating waveguide structures," *IEEE J. Quantum Electron.*, vol. 33, pp. 2038–2059, 1997.

[6] S. S. Wang, R. Magnusson, J. S. Bagby, and M. G. Moharam, "Guided-mode resonances in planar dielectric-layer diffraction gratings," *J. Opt. Soc. Am. A*, vol. 7, no. 8, p. 1470, 1990.

[7] S. Tibuleac and R. Magnusson, "Diffractive narrow-band transmission filters based on guided-mode resonance effects in thin-film multilayers," *IEEE Photonics Technol. Lett.*, vol. 9, pp. 464–466, 1997.

[8] M. R. Saleem, S. Honkanen, and J. Turunen, "Thermal properties of TiO 2 films fabricated by atomic layer deposition," *IOP Conf. Ser. Mater. Sci. Eng.*, vol. 60, p. 12008, Jun. 2014.

[9] S. Thurman and G. M. Morris, "Controlling the Spectral Response in Guided-Mode Resonance Filter Design," *Appl. Opt.*, vol. 42, no. 16, p. 3225, 2003.

Chapter 4

HYBRID DESIGN OF GMRF AND SILICON (Si) SOLAR CELL

The performance of a solar cell strongly depends on the amount of photon absorption within the cell material. A simple solar cell only absorbs those photons that meets the energy band gap value of cell material. Efficient photon absorption phenomenon in solar cells is necessary to improve their performance. In literature, many techniques have been developed to increase solar cells efficiency, as described in chapter 1. Though all these techniques revamp the absorption efficiency of solar cells, the most effective light-trapping approach is yet to be recognized. In this chapter, we report a new concept of hybrid design of guided mode resonance filter (GMRF) and silicon (Si) solar cell. GMRF is a waveguide grating structure which enables the input light to resonate multiple times within the active region of solar cell, eventually improving the absorption of light within the Si solar cell due to increase in optical path lengths. This elongation in optical path lengths allows the low energy photons to absorb in the active region and thus, improves the electrical performance of a Si solar cell.

4.1 GMR enabled Si solar cell

The guided-mode resonance (GMR) phenomenon described in chapter 3 allows the trapped light to be utilized by the integrated Si solar cell to improve the of absorption of light efficiently [1]. In this thesis work, we proposed an idea of improving absorption of light in silicon (Si) solar cells by utilizing GMR concept. The phase matching element of GMRF structure enables the incoming light to experience multiple resonances to increase the probability of light confinement within the cell material, whereas, a simple solar cell does not show absorption of light such as in GMRF structure. In a planar Si solar cell, most of the incident light wasted due to reflection and scattering losses over the top of the solar cell, which eventually decreases the efficiency of the cell [2]. While GMRF structure reduces the scattering, and reflecting loss of light by providing interfaces to the incoming light to propagate and trap within the cell material [3, 4]. For this

purpose, a hybrid design of GMRF structure with Si solar cell is designed in the Finite Difference Time Domain (FDTD) software.

4.2 Hybrid design of GMRF with Si solar cell

Figure 4.1, illustrates the schematic representation of the hybrid design. Such hybrid structure is designed by a sub-wavelength grating structure of SiO_2 coated with a thin layer of TiO_2 and then integrated with a silicon (Si) solar cell of 500 nm in thickness (T). The hybrid device is designed in the FDTD designer. TE-polarized light is incident on the top of the hybrid structure and a resonance peak occurs at a resonance wavelength of λ_r = 632.8 nm. The resonated light traps in the active region and ultimately enhances the photon elongation path within the silicon solar cell so that even low energy photons get enough energy to excite electrons in the active layer of solar cell [5]. Hence, increases the power transformation capability of the Si solar cell.

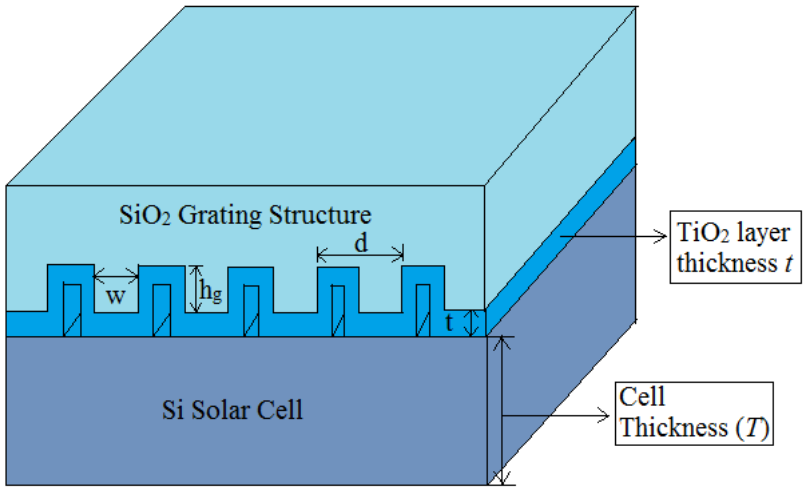

Figure 4.1: Schematic view GMRF enabled Si solar cell hybrid device with parameters; TiO_2 layer thickness t = 50 nm, grating period d = 316 nm, grating height h_g = 120 nm, structure-line width w = 205 nm, and Si solar cell thickness T = 500 nm [4].

The refractive index of silicon material at a resonance wavelength of 632.8 nm is a complex value i.e., $N = n + ik$, where n symbolizes the real value and k which is called as extinction coefficient, symbolizing the imaginary part of the refractive index. In our design, we have designed the silicon (Si) solar cell to operate in a wavelength range of 400-1100 nm with an energy band-gap of 1.1 eV [6]. Figure 4.2, illustrates the refractive-index distribution for the

hybrid device in the FDTD designer; refractive index of a material controls the propagation of light within the material. The complex refractive index value of Si material at λ_r = 632.8 nm is $N = 3.882 + \mathrm{i}(0.019)$ as shown in Figure 4.2.

4.2.1 Design and simulation results of hybrid device

To show efficient light trapping mechanism of GMRF structure within silicon (Si) solar cell the simulations of hybrid design are accomplished in the FDTD simulator and analyzed in the FDTD analyzer. The effective light trapping phenomenon of resonance waveguide SiO_2 grating structure coated with TiO_2 thin layer is demonstrated in Figure 4.3, (the index 1 on the palette shows 100% intensity of light in the figure). Figure 4.4(a) and (b), illustrates the comparison between the propagation of light in GMRF enabled Si solar cell and a planar Si solar cell. The light confinement in hybrid structure design is quite prominent in contrast to simple Si solar cell. The light absorption phenomenon within a solar cell is strongly dependent on the energy of photons coming in the incident light [7, 8].

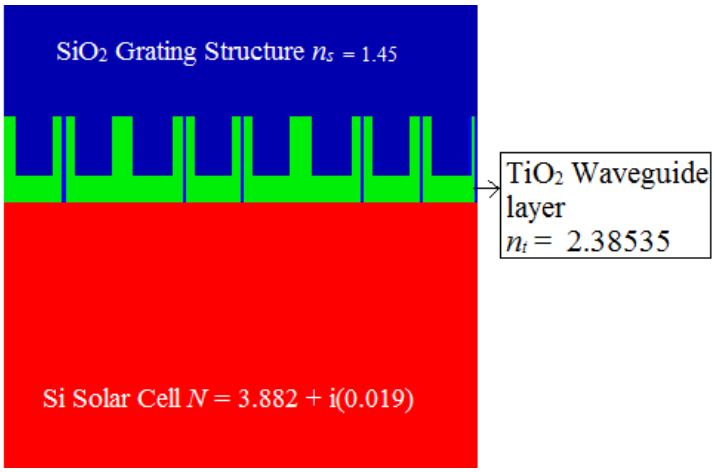

Figure 4.2: Design of refractive-index distribution of hybrid device in the FDTD designer [4].

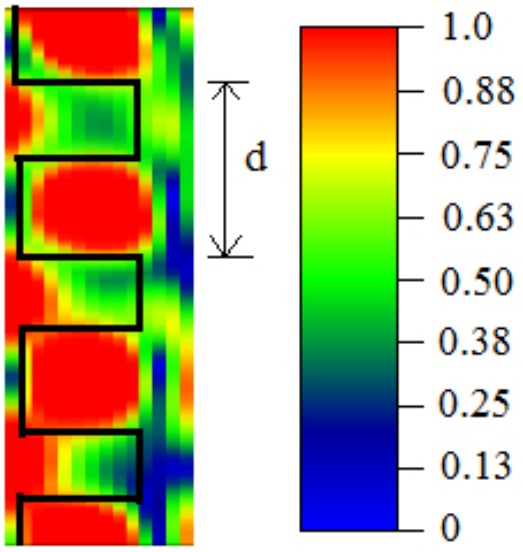

Figure 4.3: Simulation result of GMRF structure with parameters; TiO_2 layer thickness t = 50 nm, grating period d = 316 nm, grating height h_g = 120 nm, line-width w = 205 nm, incident angle $\theta_i = 18^o$, resonance wavelength λ_r = 632.8 nm, refractive index of TiO_2 n_t = 2.385, refractive index of SiO_2 n_s = 1.45, and fill factor f = 0.65 [4].

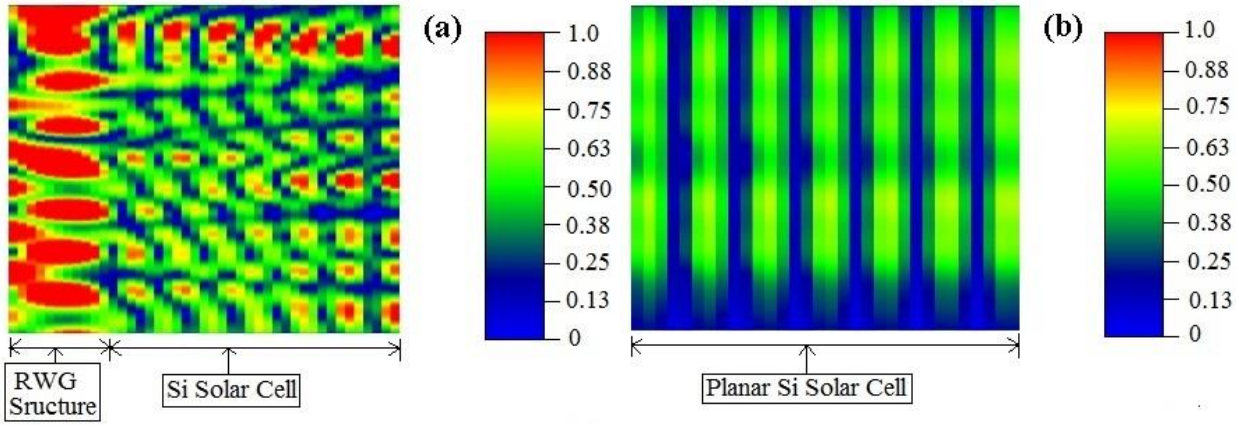

Figure 4.4: Propagation of light at resonance wavelength λ_r = 632.8 nm (a) in a hybrid device structure (b) in a planar Si solar cell. The direction of propagation of light is from left to right in figures (a) and (b) [4].

4.2.2 Optical Absorption

The absorption efficiency of a solar cell critically depends on the absorption coefficient α of the solar cell material. The length of penetration of a light at a particular wavelength in a material is directly dependent on the absorption coefficient, the more the value of α, the more will be the absorption efficiency [9], whereas the absorption coefficient of a

material depends on the wavelength of the incoming light and extinction coefficient *k* of the respective material which is the imaginary part of the complex refractive index of the material [10]. The absorption coefficient is given by the equation,

$$\alpha = \frac{4\pi k}{\lambda}, \qquad (4.1)$$

where, λ represents the wavelength of incoming light and *k* is the extinction coefficient. The selected value of extinction coefficient of silicon at wavelength 632.8 nm for hybrid structural design is $k = 0.019$ [6]. However, the simulation results of hybrid structural design are carried out using three different values of extinction coefficient i.e., ($k = 0$, $k = 0.019$, $k = 0.03$) of silicon material to analyze the effect of light absorption in the solar cell at designed resonance wavelength of 632.8 nm. FDTD based analysis shows an increase in absorption in the GMRF enabled Si solar cell with the increase in value of *k*. Figure 4.5, shows the simulation results at three different values of *k*, at same value of real part *n* of refractive index. Moreover, the analysis shows that increase in the extinction coefficient *k* results in decaying the electric field distribution patterns within the Si solar cell, however, in the presence of guided mode resonance (GMR) phenomenon the field patterns still exist to improve the light absorption. A gradual increase in the *k* value for silicon material shows a continuous enhancement in the absorption of light in the spectral range of 550-750 nm. Figure 4.6, illustrates the absorbance spectra of a hybrid structural design of GMRF enabled Si solar cell at three values of *k* (already defined in Figure 4.5). For $k = 0$, the absorbance spectra show about 49% absorption efficiency. The absorption efficiencies show a slight increase to 52% and 54% at $k = 0.019$ and 0.03 values, respectively. This is almost 38% enhancement over a planar silicon solar cell which shows 25% absorption efficiency [11]. This enhancement in optical absorption of solar cell activates the low energy photons to provoke the electrons from valance band to the conduction band to improve the electrical performance of a GMRF enabled Si solar cell.

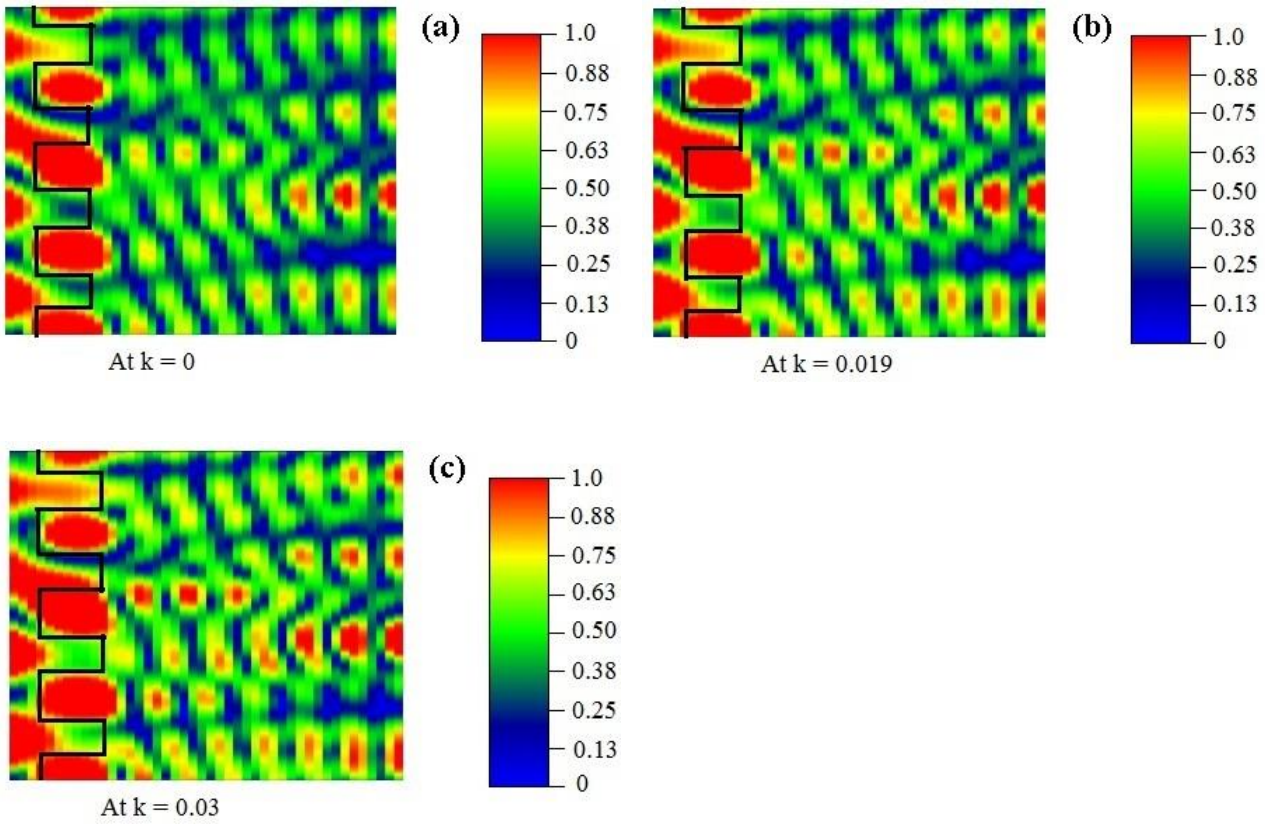

Figure 4.5: Absorption of light and electric field distribution within a hybrid structural device at resonance wavelength λ_r = 632.8 nm (a) at k = 0, (b) at k = 0.019 (original value of k at λ_r = 632.8 nm) (c) at k = 0.03. The direction of propagation of light is from left to right in figures (a), (b) and (c) [4].

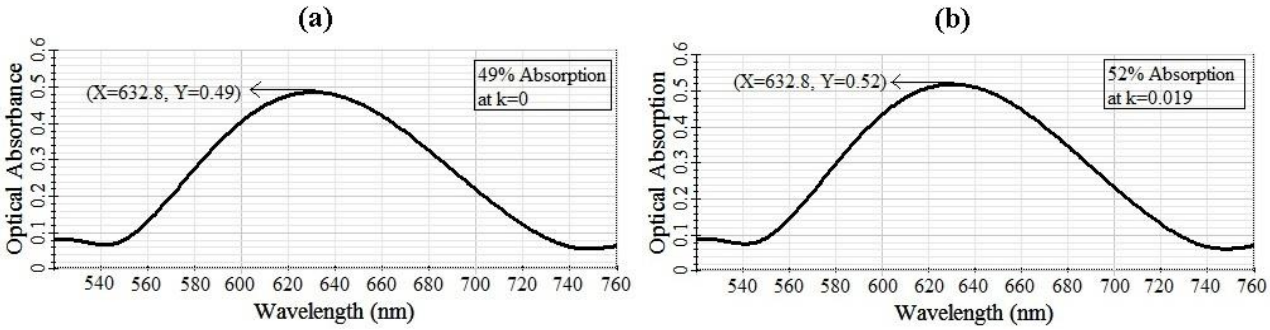

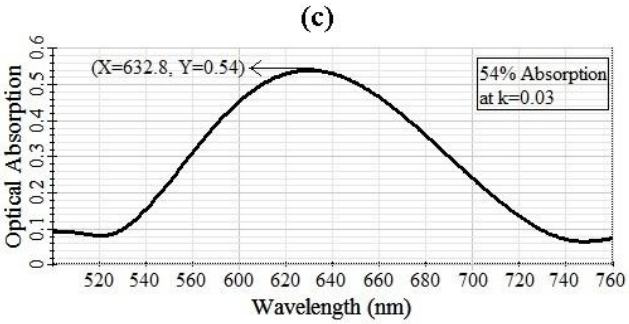

Figure 4.6: Absorbance spectra of a GMRF enabled Si solar cell at geometrical parameters of grating; d = 316 nm, h_g = 120 nm, w = 205 nm, f = 0.65, λ_r = 632.8 nm, θ_i = 18°, t = 50 nm and thickness of Si solar cell T = 500 nm. Optical absorption in Si material at (a) k = 0, (b) k = 0.019 (original value of k at λ_r = 632.8 nm), and (c) at k = 0.03 [4].

4.3 Summary

In this chapter, a hybrid structural device of guided mode resonance filter (GMRF) with silicon (Si) solar cell is established by using FDTD software. The GMRF enabled Si solar cell is designed in FDTD designer and simulations of the hybrid design are accomplished in FDTD simulator. The FDTD analyzer is used to compile the simulation results of the hybrid device. In simulations, an efficient light trapping mechanism is shown by GMRF structure at a resonance wavelength of 632.8 nm. Such effective light trapping phenomenon results in the propagation of light within the GMRF enabled Si solar cell to enhance in comparison to a planar Si solar cell. This enhancement in propagation of light increases the absorption of light in Si solar cell by providing enough energy to photons coming in incident light to harvest more electron-hole pairs within the active layer of solar cell. The dependency of absorption efficiency of a solar cell on absorption coefficient of the cell material is demonstrated through simulation results and also showed the enhancement in absorption of light by increasing the value of extinction coefficient of the cell material. The GMR effect also successfully maintained a proper electric field pattern within the Si solar cell to improve the electrical operation of the solar cell. The enhancement in the optical absorption of GMRF enabled Si solar cell is demonstrated in absorption spectra of the hybrid device. Finally, a 38% improvement in the absorption efficiency of GMRF enabled Si solar cell is calculated in comparison to a simple Si solar cell which shows 25% absorption efficiency. This enhancement in absorption efficiency of hybrid device improves the electrical performance of a Si solar cell by creating more free electrons in the conduction band of the cell material.

References

[1] M. Wellenzohn and R. Hainberger, "Light trapping by backside diffraction gratings in silicon solar cells revisited.," *Opt. Express*, vol. 20, no. 1, pp. A20-7, 2012.

[2] L. C. Hirst and N. J. Ekins-Daukes, "Fundamental losses in solar cells," *Prog. Photovoltaics Res. Appl.*, vol. 19, pp. 286–293, 2011.

[3] F. Lemarchand, a Sentenac, E. Cambril, and H. Giovannini, "Study of the resonant behaviour of waveguide gratings: increasing the angular tolerance of guided-mode filters," *J. Opt. A Pure Appl. Opt.*, vol. 1, pp. 545–551, 1999.

[4] M. S. Badar and M. R. Saleem, "Improved absorption efficiency of silicon (Si) solar cells through Resonant Waveguide Gratings (RWGs) ??? A hybrid design of RWG and Si solar cell," *Optik (Stuttg).*, vol. 128, pp. 50–56, 2017.

[5] T. Khaleque, H. G. Svavarsson, and R. Magnusson, "Fabrication of resonant patterns using thermal nano-imprint lithography for thin-film photovoltaic applications," *Opt. Express*, vol. 21, p. A631, 2013.

[6] M. a. Green, "Self-consistent optical parameters of intrinsic silicon at 300K including temperature coefficients," *Sol. Energy Mater. Sol. Cells*, vol. 92, no. 11, pp. 1305–1310, Nov. 2008.

[7] W. Wang, S. Wu, K. Reinhardt, Y. Lu, and S. Chen, "Broadband light absorption enhancement in thin-film silicon solar cells," *Nano Lett.*, vol. 10, pp. 2012–2018, 2010.

[8] R. Dewan and D. Knipp, "Light trapping in thin-film silicon solar cells with integrated diffraction grating," *J. Appl. Phys.*, vol. 106, no. 7, 2009.

[9] M. J. Keevers and M. a. Green, "Absorption edge of silicon from solar cell spectral response measurements," *Appl. Phys. Lett.*, vol. 66, no. 2, p. 174, 1995.

[10] M. a Green and M. J. Keevers, "Optical properties of intrinsic silicon at 300 K," *Prog. Photovoltaics Res. Appl.*, vol. 3, pp. 189–192, 1995.

[11] R. M. Swanson, "Approaching the 29% limit efficiency of silicon solar cells," *31st IEEE Photovoltaics Spec. Conf.*, pp. 889–894, 2005.

Chapter 5

CONCLUSIONS AND OUTLOOK

5.1 Conclusions

This thesis work provides a concept of improving the optical absorption of a silicon (Si) solar cell by employing guided-mode resonance filter (GMRF). The main goal of this concept is to efficiently trap incoming light within the active region of Si solar cell to increase the propagation lengths. The GMRF structure is a sub-wavelength waveguide grating structure allows the input light to resonate multiple times within the cell material and increases the probability of light absorption. For this purpose, a hybrid structural design of Si solar cell with GMRF is accomplished in two steps by using two different methods. In the first step, a guided mode resonance filter (GMRF) structure is designed in Fourier modal method (FMM). The GMRF structure is defined by designing sub-wavelength gratings in fused silica (SiO_2) material coated with a high index waveguide layer of amorphous titanium dioxide (TiO_2) (50 nm in thickness). At optimized design parameters, a 100% specular reflectance response of the GMRF structure is observed for both TE- polarized and TM- polarized incoming light waves at specific resonance wavelengths of 632.8 nm and 577.6 nm, respectively. By using Fourier modal analysis, the effect of variable design parameters on the specular reflectance response of the GMRF structure is successfully demonstrated and showed that spectral reflectance response can also be observed at different resonance wavelengths by varying design parameters. Hence, an efficient spectral resonance response can easily be attained by appropriate selection of optical and geometrical design parameters of GMRF structure. This versatility of GMRF structure enables them to employ for different applications in the field of optics and photovoltaics (PV). The guided-mode resonance (GMR) effect provides a new concept of hybrid design of Si solar cell and GMRF structure.

In the second step, a hybrid structure of Si solar cell with GMRF structure is designed in the FDTD software. The FDTD software comprises of three steps: firstly, the hybrid device structure is designed in FDTD designer, then in second step simulations of hybrid device is

accomplished in FDTD Simulator and finally, all the simulations are analyzed by FDTD Analyzer. During analysis of simulation results, it is observed that the GMRF structure efficiently trapped the input light and maintained a proper electric field pattern throughout the depth of silicon (Si) solar cell. Hence, the absorption coefficient of hybrid structural design is increased by employing such effective properties of GMRF structure. Thus, the simulation results of this hybrid device structure show an improvement in optical absorption to about 38% in the wavelength range of 550-750 nm for GMRF enabled Si solar cell in comparison to a planar Si solar cell. In simulation results, it is also exhibited that the absorption coefficient of Si solar cell is increased by increasing the value of extinction coefficient of Si material, eventually enhances the optical absorption of GMRF enabled Si solar cell. Such improvement in optical absorption enhances the electrical performance of solar cells by generating more free electrons in the conduction band of the cell material. This increase in number of free electrons increase the photocurrent value of Si solar cells, eventually increases the short circuit current density and open circuit voltage values of silicon (Si) solar cells.

In our study, we have analyzed the optical performance of GMRF structure by all aspects and found that GMRFs have great potential for improving the absorption efficiency of solar cells. The GMRF enabled solar cells with effective light trapping and light absorption can be fabricated by using appropriate and economical fabrication techniques. The guided-mode resonance (GMR) phenomenon actually depends on light dispersive properties and band gap of the absorbing photovoltaic materials. The GMR effect enhances the photon absorption by allowing the low energy photons to efficiently absorb inside the photovoltaic materials to improve their absorption efficiency. This improvement in optical absorption leads to enhancement in the power conversion efficiency of GMRF enabled solar cells. Hence, enhancement in absorption of light through GMRFs has a remarkable improvement on different types of solar cells such as, inorganic, organic, thin-films etc., with define material properties, structural layers, and engineering parameters. The application of GMRFs in solar cells reduces the reflection losses and improves light manipulation that can improve the performance of solar cells and hence, play a vital role in advancement of photovoltaics (PV) industry.

5.2 Outlook

The research work demonstrated in this thesis can be extended into the following research domains:

Optimized design and fabrication of GMRF enabled solar cells

The design parameters need to be optimized properly for an efficient light absorption so that a maximum number of charge carriers can be generated within nano-structured solar cells. An appropriate optimization of design parameters and structural shape is required for GMRF enabled solar cells to improve their electrical performance by increasing light absorption and effective generation of charge carriers. Low-cost efficient thin-film solar cells are the optimum goal. The reflection and scattering losses in solar cells can also be minimized by employing nanostructures of different symmetry such as, triangular shape, trapezoidal shape and rectangular shape grating structures. These structures show more trapping of light within solar cells because of their 2D structural symmetry and hence, show more enhancement in optical absorption of solar cells as compared to 1D grating structures. Also, plasmonic nano-structured gratings provide a new concept for light confinement in all types of solar cells.

GMRF enabled thin film organic solar cells

The GMRF structure effectively improved the optical absorption of silicon (Si) solar cells; this phenomenon can also be implemented for thin-film organic solar cells. By appropriate selection of design parameters and structural shape an improvement in the electrical performance of organic solar cells can be achieved by employing guided mode resonance filters. Moreover, the application of two-dimensional waveguide grating structures can further enhance the optical absorption of organic solar cells. A hybrid design of trapezoidal grating structure with small molecule organic solar cells intensify the intensity of light in active region of hybrid structure and improves the absorption efficiency of organics solar cells. The light confinement phenomenon in thin-film organic solar cells can also be enhanced by employing nanostructures of different symmetry. This asymmetrical behavior efficiently traps the incoming light result in improved absorption efficiency of thin-film organic solar cells. The cost-effective thin layer organic solar cells with better light absorption phenomenon are the optimum goal to develop the status of the current PV industry.

Application in ultra-thin film solar cells

GMRF patterns are quite feasible for enhancing the absorption efficiency of ultra-thin solar cells. The guided mode resonance filters can easily trap the incoming light within very thin films of ultra-thin solar cells and enhance their optical absorption. Hence, improve the electrical power of ultra-thin film solar cells. Another technique to enhance the absorption efficiency is to use high-index dielectric materials to design GMRF structures with thin layer solar cells. Moreover, a hybrid structural design of periodic metallic gratings with dielectric gratings within the ultra-thin layer solar cells dramatically enhances the optical absorption of the respective solar cells. This concept of hybrid design of dual grating structures with solar cells allows the input light to couple both with plasmonic and photonic modes. Thus, increase in modes interaction enhances the photocurrent of the hybrid device as contrasted to a solar cell with single grating structure. By using optimized fabrication techniques these hybrid structures can also be defined in thin films of amorphous silicon material. The light absorption phenomenon in ultra-thin layer solar cells can also be enhanced by employing a new concept of ring-shaped plasmonic nanostructure gratings.

Application in Colloidal Quantum Dot (CQD) solar cells

The efficient light confinement phenomenon of GMRF structure can effectively improves the optical absorption of colloidal quantum dot (CQD) solar cells. The low efficiency of CQD solar cells can be efficiently enhanced by applying appropriate resonant waveguide grating structures. The guided mode resonance (GMR) phenomenon of the waveguide grating structure elongates the optical path length within the active layer of CQD solar cells, eventually improves the optical absorption. The application of nanostructured dielectric diffraction gratings in CQD solar cells effectively enhances the light absorption. The grating structure can be defined both in 1D and 2D arrangements for better light absorption. This can be achieved by appropriate selection of design parameters and fabrication techniques.